

# Lactate regulates cell cycle by remodelling the anaphase promoting complex

<https://doi.org/10.1038/s41586-023-05939-3>

Received: 21 November 2021

Accepted: 10 March 2023

Published online: 15 March 2023

 Check for updates

Weihai Liu<sup>1,2,3,10</sup>, Yun Wang<sup>1,2,4,10</sup>, Luiz H. M. Bozi<sup>1,2,10</sup>, Patrick D. Fischer<sup>1,5,6,10</sup>, Mark P. Jedrychowski<sup>1,2</sup>, Haopeng Xiao<sup>1,2</sup>, Tao Wu<sup>7</sup>, Narek Darabedian<sup>1,2</sup>, Xiadi He<sup>1,2,5</sup>, Evanna L. Mills<sup>1,2</sup>, Nils Burger<sup>1,2</sup>, Sanghee Shin<sup>1,2</sup>, Anita Reddy<sup>1,2</sup>, Hans-Georg Sprenger<sup>1,2</sup>, Nhien Tran<sup>1,2</sup>, Sally Winther<sup>1,2</sup>, Stephen M. Hinshaw<sup>8</sup>, Jingnan Shen<sup>3</sup>, Hyuk-Soo Seo<sup>1,5</sup>, Kijun Song<sup>1</sup>, Andrew Z. Xu<sup>1</sup>, Luke Sebastian<sup>1</sup>, Jean J. Zhao<sup>1,5,9</sup>, Sirano Dhe-Paganon<sup>1,5</sup>, Jianwei Che<sup>1</sup>, Steven P. Gygi<sup>2</sup>, Haribabu Arthanari<sup>1,5</sup> & Edward T. Chouhan<sup>1,2</sup>✉

Lactate is abundant in rapidly dividing cells owing to the requirement for elevated glucose catabolism to support proliferation<sup>1–6</sup>. However, it is not known whether accumulated lactate affects the proliferative state. Here we use a systematic approach to determine lactate-dependent regulation of proteins across the human proteome. From these data, we identify a mechanism of cell cycle regulation whereby accumulated lactate remodels the anaphase promoting complex (APC/C). Remodelling of APC/C in this way is caused by direct inhibition of the SUMO protease SENP1 by lactate. We find that accumulated lactate binds and inhibits SENP1 by forming a complex with zinc in the SENP1 active site. SENP1 inhibition by lactate stabilizes SUMOylation of two residues on APC4, which drives UBE2C binding to APC/C. This direct regulation of APC/C by lactate stimulates timed degradation of cell cycle proteins, and efficient mitotic exit in proliferative human cells. This mechanism is initiated upon mitotic entry when lactate abundance reaches its apex. In this way, accumulation of lactate communicates the consequences of a nutrient-replete growth phase to stimulate timed opening of APC/C, cell division and proliferation. Conversely, persistent accumulation of lactate drives aberrant APC/C remodelling and can overcome anti-mitotic pharmacology via mitotic slippage. In sum, we define a biochemical mechanism through which lactate directly regulates protein function to control the cell cycle and proliferation.

A high rate of lactate production from glucose, despite available oxygen for mitochondrial respiration, is a hallmark of rapid cellular proliferation. This metabolic phenomenon, known as aerobic glycolysis, has long been associated with proliferating cancer cells and tumours<sup>1,2</sup>. In addition, many proliferating non-transformed cell types and micro-organisms engage in aerobic glycolysis<sup>3–6</sup>, indicating that it is a general metabolic phenotype of proliferation. The proximal consequence of glycolysis is the generation of ATP and lactate, and lactate production coincides with the regeneration of cytosolic NAD<sup>+</sup>. ATP and NAD<sup>+</sup> are limiting for many biosynthetic reactions that are required for cellular growth and division<sup>7,8</sup>. Therefore, lactate production rates are highly correlated with rates of cellular anabolism and proliferation. Once produced, lactate is exported from the cell, the rate of which depends on the abundance of plasma membrane monocarboxylate transporters<sup>9</sup> (MCTs). Once secreted, lactate can act as an important source of pyruvate in many biological settings<sup>10,11</sup>. Depending on the relative rates of lactate production and secretion, intracellular lactate

concentration<sup>12–14</sup> can range from around 2 mM to more than 30 mM. Although high abundance of intracellular lactate is a measure of cellular proliferation, whether accumulated lactate can directly regulate processes involved in proliferation is not known. More generally, mechanisms through which protein function can be directly modified by accumulated intracellular lactate remain unknown. Here, we explore these questions, and identify a mechanism of metabolic regulation initiated by accumulation of the metabolic end-product of glycolysis (Extended Data Fig. 1a).

## Lactate regulates the composition of APC/C

We began by deploying an approach to identify direct effects of increased lactate abundance across the proteome. To do so, we applied thermal proteomic profiling (TPP), which uses mass spectrometry to systematically assess changes in protein thermostability. TPP is based on the phenomenon of protein denaturation upon heating leading to

<sup>1</sup>Department of Cancer Biology, Dana-Farber Cancer Institute, Boston, MA, USA. <sup>2</sup>Department of Cell Biology, Harvard Medical School, Boston, MA, USA. <sup>3</sup>Department of Musculoskeletal Oncology, The First Affiliated Hospital, Sun Yat-sen University, Guangzhou, China. <sup>4</sup>Hospital of Stomatology, Guanghua School of Stomatology, Sun Yat-sen University, Guangzhou, China.

<sup>5</sup>Department of Biological Chemistry and Molecular Pharmacology, Harvard Medical School, Boston, MA, USA. <sup>6</sup>Department of Pharmacy, Pharmaceutical and Medicinal Chemistry, Saarland University, Saarbrücken, Germany. <sup>7</sup>Department of Systems Biology, Harvard Medical School, Boston, MA, USA. <sup>8</sup>Stanford Cancer Institute, School of Medicine, Stanford University, Stanford, CA, USA. <sup>9</sup>Broad Institute of Harvard and MIT, Cambridge, MA, USA. <sup>10</sup>These authors contributed equally: Weihai Liu, Yun Wang, Luiz H.M. Bozi, Patrick Fischer. ✉e-mail: edwardt\_chouhan@dfci.harvard.edu

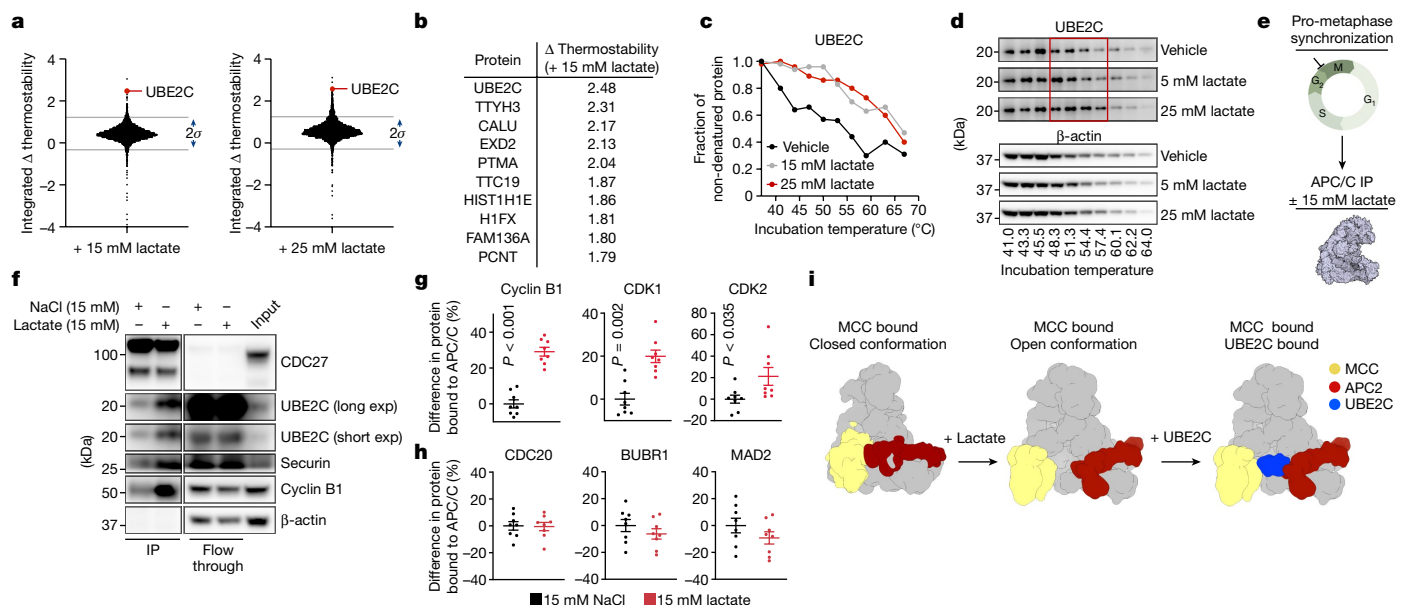


**Fig. 1 | Lactate regulates protein interactions of APC/C.** **a**, The distribution of thermostability changes in the proteome of HEK 293 cells following treatment with 15 mM and 25 mM lactate. The integrated change in thermostability ( $\Delta$  thermostability) is calculated as the sum difference in non-denatured protein across the entire temperature curve. Raw data are presented in Supplementary Table 1. **b**, The top 10 proteins exhibiting increased thermostability following treatment with 15 and 25 mM lactate in lysates of HEK 293 cells. The integrated  $\Delta$  thermostability is calculated as the sum difference in non-denatured protein across the entire temperature curve. **c**, Lactate-mediated changes in thermostability of UBE2C following treatment with 15 and 25 mM lactate in lysates of HEK 293 cells, as determined by TPP with mass spectrometry (TPP-MS). **d**, Lactate-mediated changes in thermostability of UBE2C following treatment with lactate in HeLa S3 lysates, as determined by immunoblotting. Representative blot from three experiments. **e**, Workflow for the isolation of

pro-metaphase APC/C. IP, immunoprecipitation. **f**, Immunoprecipitation of pro-metaphase APC/C (via CDC27) following treatment with 15 mM lactate in cell lysates in the presence of exogenous UBE2C demonstrates lactate-mediated binding of UBE2C, cyclin B1 and securin to pro-metaphase APC/C. Representative blot from three experiments. Exp, exposure. **g**, Immunoprecipitation with mass spectrometry (IP-MS) of APC/C (via CDC27) following treatment with 15 mM lactate in cell lysates demonstrates lactate-mediated binding of cyclin B1, CDK1 and CDK2 to APC/C.  $n = 8$  cell replicates. Two-tailed Student's *t*-test for pairwise comparisons. **h**, IP-MS of APC/C (via CDC27) following lactate treatment in cell lysates shows that there is no effect on the interaction with the MCC.  $n = 8$  cell replicates. **i**, Model of APC/C remodelling to accommodate UBE2C binding following exposure to increased lactate concentration. Schematics are based on published structures of APC/C in closed and open conformations<sup>19,30</sup>. Data are mean  $\pm$  s.e.m.

insolubility, which is used to generate melting curves for proteins. Melting curve characteristics can be altered by changes to the protein, including binding to a small molecule, post-translational modification or changes in protein–protein interactions<sup>15</sup>.

Here we applied TPP to identify proteins that exhibit altered thermostability in direct response to increased lactate abundance (Extended Data Fig. 1b). We treated lysates of native human embryonic kidney cells with vehicle, 15 mM sodium L-lactate (hereafter referred to as lactate) or 25 mM lactate for 15 min before analysis by TPP (Extended Data Fig. 1c,d). We treated diluted cellular lysates to examine direct effects of lactate, as opposed to indirect metabolic consequences of endogenous lactate metabolism in intact cells. Following treatment, native proteomes were subjected to a thermal gradient and the non-denatured fractions were collected (Extended Data Fig. 1e). Non-denatured fractions were digested by trypsinolysis and analysed by tandem mass tag (TMT)-based quantitative proteomics, which enables simultaneous quantification of the melting curve for thousands of proteins in a single experiment<sup>15</sup> (Extended Data Fig. 1e and Supplementary Table 1). In doing so, we monitored lactate-dependent changes in thermostability for more than 3,900 proteins (Fig. 1a). Of the detected protein population, fewer than 1% exhibited a consistent increase in thermostability in response to both 15 mM and 25 mM lactate (Fig. 1a,b and Supplementary Table 1). Among the proteins exhibiting the most robust shift in thermostability was UBE2C (Fig. 1a–c). We confirmed these results by targeted analysis of UBE2C in cellular lysates across multiple cell types (Fig. 1d, Extended Data Fig. 1f and Supplementary Fig. 1). Contrastingly, equivalent concentrations of

D-lactate or pyruvate caused no detectable change in UBE2C thermostability (Extended Data Fig. 1g).

UBE2C is an E2 enzyme and a transient binding partner of the anaphase promoting complex (APC/C), which is required to facilitate APC/C-mediated ubiquitylation of cyclin B1 and securin<sup>16,17</sup>. The ubiquitylation of cell cycle proteins in this manner causes their degradation and is a major control point in the metaphase-to-anaphase transition and mitotic exit<sup>18</sup>. UBE2C recruitment to APC/C requires structural reorganization of APC/C subunits to mediate UBE2C binding<sup>19</sup>—the mechanisms regulating this timed remodelling are not fully defined<sup>20,21</sup>. Given the central importance of UBE2C in cell cycle regulation, we sought to understand the basis for lactate-mediated increases in its thermostability. On the basis of the large absolute increase in UBE2C thermostability (Fig. 1a–c), we reasoned that these effects were probably not a consequence of direct lactate binding, since low-affinity small molecule interactions do not typically manifest large shifts in these parameters<sup>22</sup>. Moreover, we observed no detectable post-translational modifications of UBE2C protein or changes in UBE2C abundance due to lactate treatment (Extended Data Fig. 1h,i).

Large shifts in protein thermostability can result from acquired protein–protein interactions<sup>15</sup>. For this reason, we explored whether lactate could regulate UBE2C engagement with its binding partner APC/C. To do so, we first treated cells with thymidine and nocodazole to achieve synchronization in pro-metaphase (Fig. 1e). At this stage of the cell cycle, APC/C is bound to the mitotic checkpoint complex (MCC) and not UBE2C<sup>23,24</sup>. We next treated lysates from synchronized cells with or without 15 mM lactate for 15 min before immunoprecipitation

# Article

of APC/C. As expected, immunoprecipitation of APC/C in the presence of exogenous UBE2C detected minimal interaction, indicative of the pro-metaphase conformation of APC/C being incompatible with UBE2C binding<sup>23,24</sup> (Fig. 1f). However, incubation of lysates with 15 mM lactate was sufficient to substantially increase UBE2C binding to APC/C (Fig. 1f). Cyclin B1 and securin are major cell cycle regulators that are recruited to the UBE2C-bound form of APC/C<sup>10</sup>. Treatment with 15 mM lactate also increased the binding of both factors to pro-metaphase APC/C (Fig. 1f). Similarly, acute treatment of cell lysates with lactate was sufficient to drive binding of endogenous UBE2C to APC/C (Extended Data Fig. 1j). Conversely, immunoprecipitation of UBE2C from cell lysates also resulted in increased binding to APC/C following lactate treatment (Extended Data Fig. 1k). The degree of UBE2C, cyclin B1 and securin binding to APC/C was quantitatively responsive to lactate across a 5–15 mM range (Fig. 1f and Extended Data Fig. 1l). By contrast, cell lysates treated with 15 mM D-lactate or pyruvate resulted in no effect on the binding of UBE2C, securin or cyclin B1 to APC/C (Extended Data Fig. 1m).

We next assessed more broadly how APC/C-interacting proteins were remodelled following incubation with lactate. We performed immunoprecipitation of APC/C with or without lactate addition, as above, followed by mass spectrometry analysis of the interacting proteins. In doing so, we identified increased binding of CDK1 and CDK2 to APC/C, both of which are binding partners of cyclin B1<sup>25,26</sup> (Fig. 1g and Supplementary Table 2). By contrast, treatment with 15 mM D-lactate or pyruvate caused no alterations to the profile of these APC/C-interacting proteins (Extended Data Fig. 1n). Additionally, we observed no change in abundance of MCC components due to lactate (Fig. 1h and Supplementary Table 2). Together, our data indicate that acute exposure to high concentrations of lactate is sufficient to remodel APC/C to accommodate UBE2C binding and produce a conformation primed for ubiquitylation of cyclin B1 and securin (Fig. 1i).

## Lactate increases SUMOylation of APC4

We next investigated how lactate could remodel the composition of APC/C to promote UBE2C binding. We examined several post-translational modifications by mass spectrometry and found no evidence for lactate-dependent changes to any APC/C components (Extended Data Fig. 1o,p and Supplementary Table 3). However, in performing mass spectrometry analysis of APC/C, we observed lactate-dependent increases in SUMO2 and SUMO3 (SUMO2/3) conjugation (Fig. 2a,b). Proteins that regulate SUMOylation are essential for mitotic progression<sup>27</sup>. Moreover, APC4 can be SUMOylated at two C-terminal residues, and these modifications are required for timely anaphase onset<sup>28,29</sup>. In addition, APC4 SUMOylation has been shown to reposition the WHB domain of APC2, enabling more efficient activation of APC/C<sup>30</sup>. However, the mechanisms controlling timed SUMOylation of APC4 to facilitate the activation of APC/C in this way are not known. We were curious to understand whether lactate stabilized SUMOylation of APC/C subunits and whether these modifications were relevant for lactate-mediated remodelling of APC/C.

Following treatment of pro-metaphase cell lysates with or without 15 mM lactate, purification of APC/C revealed increased SUMOylation of a single protein with a molecular mass corresponding to APC4 (Fig. 2c). We immunopurified APC4 directly, and showed that lactate specifically increased SUMO2/3 on a protein with the molecular mass of APC4 (Fig. 2d). The mass shift suggested that two residues on APC4 were SUMOylated. Intact cells synchronized at pro-metaphase and treated with lactate also exhibited increased SUMOylation of a protein with the molecular mass of APC4 (Fig. 2e). We observed a comparatively modest stabilization of SUMO1 at this molecular mass (Extended Data Fig. 1q). By contrast, cell lysates treated with 15 mM D-lactate or pyruvate exhibited no effect on APC4 SUMOylation (Fig. 2f).

Increased lactate did not broadly affect the amount of bulk protein SUMOylation (Extended Data Fig. 2a). To examine the breadth

of lactate-mediated effects on protein SUMOylation in more detail, we monitored alterations in SUMO2/3 substrates proteome-wide following treatment with or without 15 mM lactate (Extended Data Fig. 2b and Supplementary Table 4). Out of 860 proteins that we profiled, 16 exhibited significant increases in SUMO2/3 binding following lactate treatment (Extended Data Fig. 2b,c). Together, these data suggested a targeted effect of lactate on the SUMO2/3 pathway, the basis of which is explored in a later section. We next defined the sites of lactate-dependent SUMOylation on APC4. Previous studies indicated that APC4 K772 and K798 can be SUMOylated<sup>28,29</sup>. We engineered cells expressing a mutant APC4 that could not be SUMOylated at these sites (APC4(K772/798R)) (Extended Data Fig. 2d–h). Lactate-dependent SUMOylation of APC4 was completely abrogated in cells expressing APC4(K772/798R), indicating that these sites were the SUMO2/3 targets on APC4 (Fig. 2g,h).

We next examined whether SUMOylation of APC4 is required for lactate-mediated reorganization of APC/C and UBE2C binding. Lactate-mediated binding of UBE2C to APC/C was completely abrogated in cells expressing APC4(K772/798R) (Fig. 2i). Additionally, the lactate-dependent increase in cyclin B1 and securin binding to APC/C was prevented in cells expressing APC4(K772/798R) (Extended Data Fig. 2i). Together, these findings demonstrate that high lactate concentrations increase UBE2C binding to APC/C by increasing SUMOylation of APC4. Moreover, these data indicate that a proximal consequence of APC4 SUMOylation is a structural reorientation of APC/C to accommodate UBE2C binding. Notably, APC2 possesses a SUMO-interacting motif proximal to APC4<sup>30</sup>. On the basis of recent structures of APC/C, the APC2 SUMO-interacting motif is directly adjacent to the APC2 WHB domain, which accommodates UBE2C binding<sup>21,30</sup>. We therefore propose a model whereby a direct consequence of lactate-mediated SUMOylation of APC4 is a reorientation of APC4–APC2 interactions via APC4–SUMO2/3 and the APC2 SUMO-interacting motif. This structural reorganization provides an APC2 orientation that is permissive for UBE2C binding (Fig. 2j).

## Lactate and zinc complex in SENP1

We next determined the direct mechanistic target of lactate that could explain the lactate-mediated increase in APC4 SUMOylation. We first considered the fact that lactate increased APC4–SUMO2/3 in the absence of bulk changes to protein SUMOylation in the cell (Fig. 2a–e and Extended Data Fig. 2a), suggesting a specific interaction between the SUMO pathway and APC4. Steady-state levels of protein SUMOylation are typically low owing to high activity of deSUMOylating enzymes, in particular sentrin isopeptidases<sup>31</sup> (SENP1s). Within the SENP family, SENP1 has a major role in mitotic progression and can reduce SUMOylation of APC4<sup>28,32</sup>. On this basis, we hypothesized that SENP1 could be a direct inhibitory target of lactate, leading to stabilization of APC4 SUMOylation. In support of this hypothesis, we found that genetic depletion of SENP1 fully recapitulated the effects of increased lactate. Knockout of SENP1 increased APC4 SUMOylation (Fig. 3a and Extended Data Fig. 2j) and increased the binding of UBE2C to APC/C (Fig. 3b). Moreover, an increase in lactate in SENP1-KO cells resulted in no further increase in APC4 SUMOylation (Extended Data Fig. 2k,l). Thus, lactate-mediated elevation of APC4–SUMO2/3 requires SENP1.

On the basis of these findings, we hypothesized that lactate somehow inhibits SENP1 activity to stabilize SUMOylation on APC4. To consider the mechanistic basis for such a model, we examined the structural features of SENP1. The active site of human SENP1 contains a catalytic triad characteristic of cysteine proteases, consisting of Cys603, His533 and Asp550. Unusually, SENP1 also possesses an additional Cys535 in the active site (Fig. 3c). We noted that the structural features of the SENP1 active site were similar to pockets that possess the capacity to bind zinc. Examining the structure of the SENP1 catalytic domain using the ZincBind algorithm<sup>33</sup> indicated that several residues exhibited

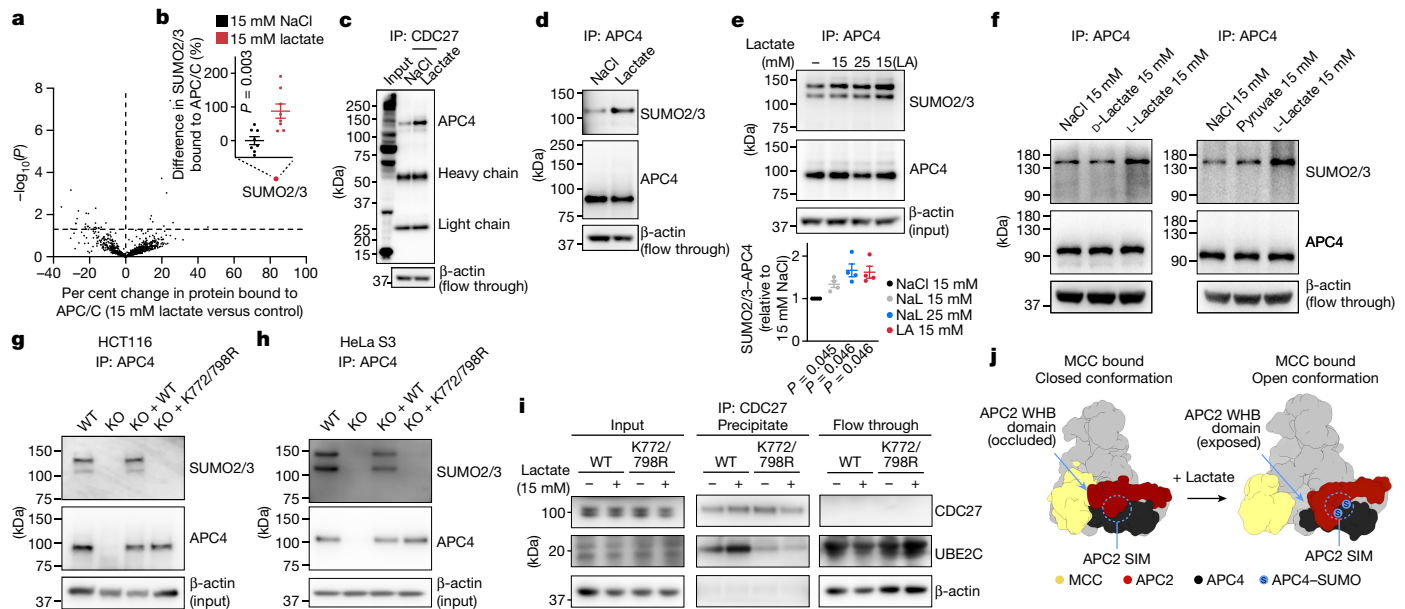


**Fig. 2 | Lactate regulates APC/C composition via SUMOylation of APC4.**

**a**, IP-MS of APC/C (via CDC27) following lactate treatment in cell lysates.  $n = 8$  cell replicates. **b**, Quantification of the change in SUMO2/3 association with APC/C proteins following exposure to lactate in cell lysates, via mass spectrometry.  $n = 8$  cell replicates. Two-tailed Student's *t*-test for pairwise comparisons. **c**, SUMO2/3 immunoblot of immunopurified APC/C (via CDC27) following lactate treatment in cell lysates. An immunoreactive band is indicated at the molecular mass of SUMOylated APC4. Representative blot from three experiments. **d**, SUMO2/3 immunoblot of immunopurified APC4 following lactate treatment in cell lysates. Representative blot from two experiments. **e**, SUMO2/3 immunoblot of immunopurified APC4 following lactate treatment in intact cells for 4 h. Bottom, densitometry analysis of immunoblots. Representative blot from four experiments. One-way ANOVA with Bonferroni's post hoc test for multiple comparisons. NaL, sodium lactate; LA, lactic acid.

**f**, SUMO2/3 immunoblot of immunopurified APC4 following D-lactate, pyruvate or L-lactate treatment in cell lysates. Representative blot from three experiments. **g,h**, SUMO2/3 immunoblot of immunopurified APC4 from HCT116 (**g**) and HeLa S3 (**h**) wild-type (WT) and APC4-knockout (KO) cells, and cells expressing APC4(K772/798R); 15 mM lactate was added to all lysates. **i**, Immunoprecipitation of pro-metaphase APC/C (via CDC27) following lactate treatment in cell lysates demonstrates that lactate-mediated binding of UBE2C to pro-metaphase APC/C requires the APC4 SUMO2/3 target residues K772 and K798. Representative blot from three experiments. **j**, Model of APC/C remodelling to accommodate UBE2C binding following lactate-mediated stabilization of SUMO2/3 on APC/C. Schematics are based on published structures of APC/C in closed and open conformations<sup>19</sup>, with and without SUMOylation<sup>30</sup>. SIM, SUMO-interacting motif. Data are mean  $\pm$  s.e.m.

properties that favour zinc coordination (Extended Data Fig. 2m). Furthermore, molecular modelling of zinc binding to SENP1 indicated the side chains of His533, Cys535, Asp550 and the backbone carbonyl of Trp534 form a favourable tetrahedral coordination with the Zn<sup>2+</sup> ion (Fig. 3c). In this binding mode, the catalytic Cys603 is displaced from its native electronic environment. We hypothesized that this configuration might be amenable to further stabilization of Zn<sup>2+</sup> at the SENP1 active site. In light of this idea, we considered the fact that carboxylate groups possess the capacity to chelate protein-bound zinc. Carboxylate chemical warheads have been designed to coordinate zinc within proteins<sup>34,35</sup>. Moreover, the capacity of the carboxylate group on lactate to chelate free zinc is known<sup>36,37</sup>. However, the biological relevance of this interaction has not been explored. On the basis of these observations, we hypothesized that at high concentrations, the lactate carboxylate group could chelate SENP1-bound zinc, which could stabilize zinc binding to the active site of SENP1.

We first determined whether zinc binds to and inhibits SENP1. We examined potential interactions between zinc, lactate and the catalytic domain of human SENP1 using NMR. A suite of transverse relaxation-optimized spectroscopy (TROSY)-based triple resonance backbone experiments recorded on [<sup>2</sup>H, <sup>13</sup>C, <sup>15</sup>N]-labelled SENP1 allowed for assignment of 88% of non-proline residues (Supplementary File 1 and Supplementary Table 5). Addition of ZnSO<sub>4</sub> to SENP1 led to significant broadening of 32 resonances in the <sup>1</sup>H, <sup>15</sup>N-TROSY-HSQC spectrum, indicating binding and/or conformational change to the corresponding residues in an intermediate exchange regime (Extended Data Fig. 3a and Supplementary File 1). Significant intensity reduction was localized entirely in direct proximity

to the active site (Extended Data Fig. 3b,c). Moreover, addition of lactate and zinc in combination substantially potentiated spectra shift and signal loss for a subset of these same zinc-responsive active site residues, including Cys535 (Fig. 3d,e and Extended Data Fig. 3d,e). We further confirmed the involvement of Cys535 in L-lactate–zinc binding by mass spectrometry analysis of zinc-bound SENP1 cysteines<sup>38</sup> (Extended Data Fig. 3f,g). Indeed, we observed selective coordination of SENP1 Cys535 by zinc that was potentiated by the presence of L-lactate (Fig. 3f and Extended Data Fig. 3g). Conversely, stabilization of zinc binding to SENP1 Cys535 was not achieved with D-lactate or pyruvate (Fig. 3f). Moreover, addition of D-lactate or pyruvate to zinc-bound SENP1 resulted in no detectable chemical shift perturbations (CSPs) to the active site residues of the SENP1 <sup>1</sup>H, <sup>15</sup>N-HSQC spectra, when compared to L-lactate (Extended Data Fig. 3h,i). Additionally, incubation of L-lactate without zinc resulted in no detectable CSPs to the active site residues of the SENP1 <sup>1</sup>H, <sup>15</sup>N-HSQC spectra (Extended Data Fig. 3j).

We next examined the effects of L-lactate and zinc on the deSUMOylation activity of recombinant SENP1. Zinc alone inhibited SENP1 activity, exhibiting a half-maximal inhibitory concentration (IC<sub>50</sub>) of 280 nM (Fig. 3g and Extended Data Fig. 4a,b). This effect was not observed with other divalent cations at respective physiological concentrations (Extended Data Fig. 4c). L-lactate alone also had no effect on SENP1 activity (Extended Data Fig. 4d). However, L-lactate and zinc in combination lowered the IC<sub>50</sub> to 23 nM (Fig. 3g and Extended Data Fig. 4b). Of note, small molecule carboxylates structurally similar to L-lactate, including D-lactate, did not affect zinc-mediated inhibition of SENP1 (Fig. 3h). Together, these data suggest that an appropriately

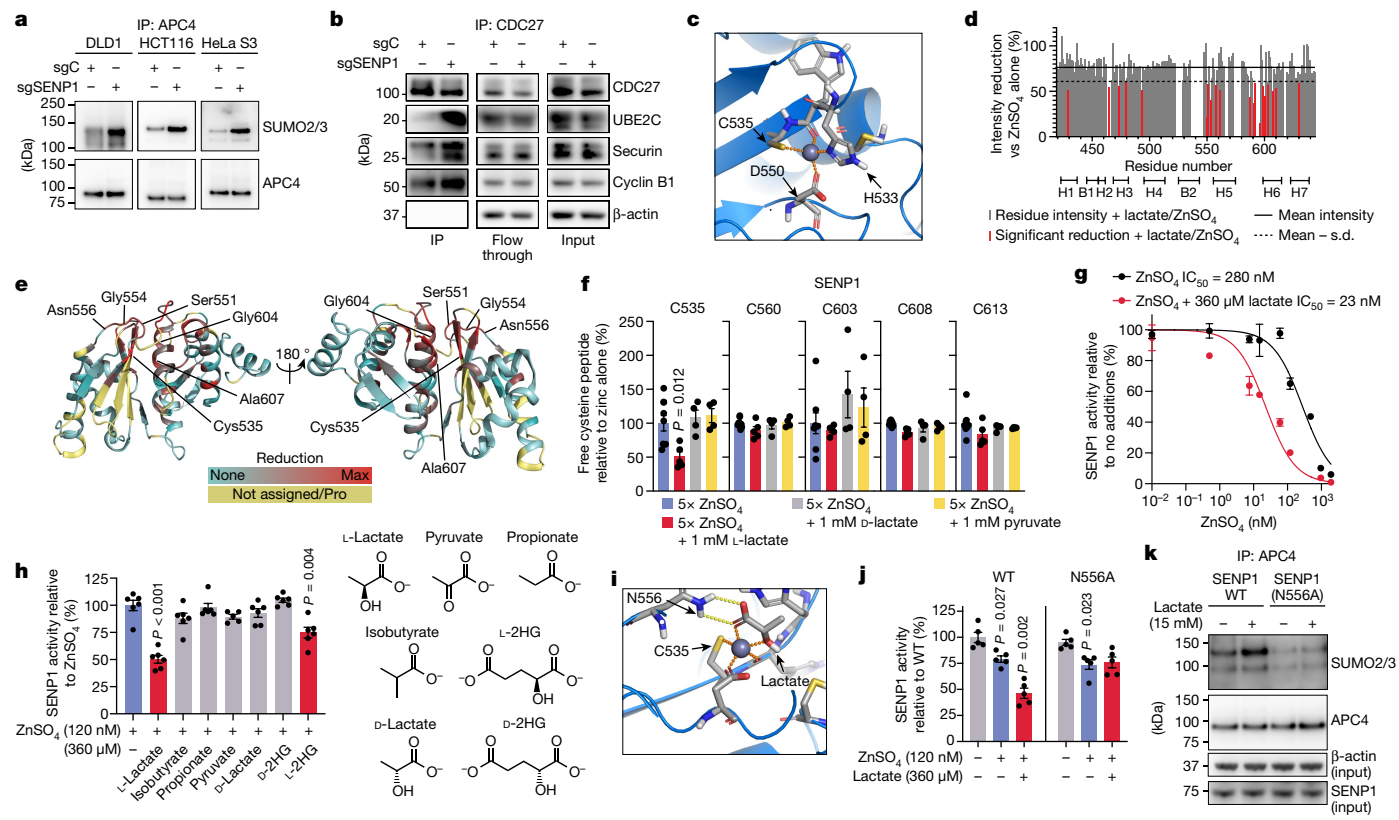


**Fig. 3 | Lactate forms a complex with zinc in the SENP1 active site to inhibit APC4 deSUMOylation.** **a**, SUMO2/3 immunoblot of immunopurified APC4 from wild-type and SENP1-KO cells. Representative blot from four experiments. sgC, control guide RNA; sgSENP1, SENP1 guide RNA. **b**, Immunoprecipitation of pro-metaphase APC/C (via CDC27) in wild-type and SENP1-KO cells in the presence of exogenous UBE2C. Representative blot from three experiments. **c**, Molecular model of the favourable binding mode of zinc in the active site of human SENP1. **d**, Intensity reduction as a function of residue number after addition of 100  $\mu$ M zinc and 1 mM L-lactate to SENP1, compared with zinc alone. **e**, SENP1 (Protein Data Bank (PDB) ID: 2IYC) colour-coded according to the peak intensity reduction caused by lactate-potentiated zinc binding compared with zinc alone. ‘Not assigned/Pro’ refers to unassigned residues or prolines. **f**, The effect of lactate, D-lactate and pyruvate on zinc binding to SENP1 cysteine

residues, quantified by mass spectrometry. Zinc alone,  $n = 9$ ; zinc + lactate,  $n = 5$ ; all other conditions,  $n = 4$  independent samples. **g**,  $IC_{50}$  of zinc on SENP1 deSUMOylation activity in the presence and absence of lactate.  $n = 6$  independent samples. **h**, The effect of monocarboxylates on zinc-mediated inhibition of SENP1 deSUMOylation activity. Pyruvate,  $n = 5$ ; all other conditions,  $n = 6$  independent samples. **i**, Molecular model of the favourable binding mode of lactate and zinc in the active site of human SENP1. **j**, The effect of  $ZnSO_4$  and lactate on deSUMOylation activity of recombinant human wild-type SENP1 and SENP1(N556A).  $n = 5$  independent samples. **k**, SUMO2/3 immunoblot of immunopurified APC4 following lactate treatment in cellular lysates from HCT116 cells expressing wild-type SENP1 or SENP1(N556A). Representative blot from three experiments. **f,h,j**, One-way ANOVA for multiple comparisons with Bonferroni’s post hoc test. Data are mean  $\pm$  s.e.m.

oriented  $\alpha$ -hydroxy group adjacent to the lactate carboxylate mediate L-lactate coordination of SENP1-bound zinc. To further examine this idea, we explored whether L-2-hydroxyglutarate (L-2HG) could affect zinc-mediated inhibition of SENP1, as it shares this structural feature with lactate. Notably, L-2HG, but not D-2HG, was capable of potentiating zinc-mediated inhibition of SENP1, albeit less effectively than L-lactate (Fig. 3h).

We next explored the structural basis for the distinct role of lactate in modulating the interaction between zinc and SENP1 Cys535. Structural modelling provided a favourable binding mode for  $Zn^{2+}$  and lactate in the SENP1 active site (Fig. 3i). Unlike zinc alone, the presence of lactate displaces the His533 side chain and chelates  $Zn^{2+}$  in its place. In addition, the lactate carboxylate forms favourable hydrogen bonds with the Asn556 side chain, presumably providing tighter complex formation. Characterizing the structural features of the SENP1 active site relevant for lactate-mediated zinc inhibition prompted us to examine other SENP family members for shared or distinguishing properties. Monitoring deSUMOylation activity across the SENP family determined an absence of lactate-driven zinc inhibition for SENP2, 3, 5, 6 and 7 (Extended Data Fig. 4e). Zinc alone was able to inhibit activity of SENP2, SENP5 and SENP6, albeit at higher concentrations and without any additional effect of lactate (Extended Data Fig. 4e). Unlike all

other SENPs, the SENP1 active site has at least two features that support the structural basis proposed for a distinct effect of lactate on SENP1 activity, including a second cysteine residue in the active site (Cys535) as well as Asn556 (Fig. 3i and Extended Data Fig. 4f).

We next determined whether the zinc and lactate interactions with SENP1 described above were required for lactate-mediated stabilization of APC4–SUMO2/3. Notably, the lactate-mediated increase in APC4–SUMO2/3 was completely abrogated in the presence of zinc chelators (Extended Data Fig. 4g). Conversely, an increase in zinc alone was sufficient to increase SUMOylation of APC4 (Extended Data Fig. 4h). Moreover, in the presence of sub-maximal effective zinc, lactate could further stabilize APC4–SUMO2/3 (Extended Data Fig. 4i,j). Finally, structure–activity relationship analysis implicated Asn556 as a key residue mediating the inhibitory effects of L-lactate on SENP1 (Fig. 3f,h,i and Extended Data Fig. 4f). To test this directly, we generated recombinant SENP1(N556A), which exhibited deSUMOylation activity similar to the wild-type protein (Fig. 3j). The activity of SENP1(N556A) was inhibited by zinc, to a similar extent as wild-type protein (Fig. 3j), consistent with a ‘zinc-only’ binding mode with Cys535 (Fig. 3c). However, SENP1(N556A) was completely insensitive to additional inhibition by lactate (Fig. 3j), indicating that this residue has a key role in lactate-driven inhibition of SENP1 in the presence of zinc. We next

generated cells expressing the mutant SENP1(N556A) (Extended Data Fig. 4k). Lactate-mediated stabilization of APC4 SUMOylation was completely lost in SENP1(N556A) cells (Fig. 3k and Extended Data Fig. 4l), demonstrating the critical importance of SENP1(N556) in lactate-driven stabilization of APC4–SUMO2/3.

It is noteworthy that the effective concentrations of lactate for the zinc-dependent effects on SENP1 are higher in cells than in experiments performed using recombinant protein. Similar differences are frequently observed between such experimental systems, and are attributable to competing interactions for the ligand, metabolism of the ligand, or the target protein existing in a cellular context that renders it less tractable to ligation<sup>39–41</sup>. Competing interactions of this type can be modelled in recombinant protein assays by introducing excess albumin, which interacts readily with numerous structurally diverse ligands, including small molecule carboxylates<sup>42</sup>. Addition of albumin to the recombinant SENP1 deSUMOylation assay shifted the minimal effective concentration of lactate substantially (Extended Data Fig. 4m), supporting the conclusion that under conditions in which there are competing interactions, inhibitory concentrations of lactate are in the physiological millimolar range.

### Lactate regulates the cell cycle via SENP1

Our findings so far describe a mechanism through which accumulated lactate remodels APC/C via inhibition of SENP1 to increase UBE2C binding. On this basis, we explored whether this function of lactate has a general role in mitotic regulation and cellular proliferation. We hypothesized that timed remodelling of APC/C during mitosis could be driven by increased lactate abundance upon mitotic entry. Owing to the significant anabolic flux that occurs immediately before mitosis<sup>43</sup>, which is inextricably tied to increased glycolytic demand and lactate production<sup>7,8</sup>, we posited that intracellular lactate accumulation is a metabolic signature of mitotic entry (Extended Data Fig. 5a).

We first determined whether intracellular lactate concentration increases before mitosis (Extended Data Fig. 5b), and whether lactate accumulation regulates mitotic progression through APC/C remodelling. Intracellular lactate concentrations in synchronized HeLa S3 and HCT116 cells increased from approximately 6 mM to 15–20 mM upon mitotic entry, indicative of an increase in glycolytic flux to lactate (Fig. 4a and Extended Data Fig. 5c). Notably, endogenous increase of lactate concentration to around 15 mM preceded the timed degradation of cyclin B1 and securin, and mitotic exit (Fig. 4a,b and Extended Data Fig. 5c). Accumulation of intracellular lactate before mitosis coincided with stable expression of major enzymes that regulate pyruvate utilization (Extended Data Fig. 5d), and there was no detectable proteome-wide evidence for protein lactylation (Extended Data Fig. 5e). The accumulation of lactate also coincided with elevated phosphorylation of pyruvate dehydrogenase E1 subunit  $\alpha$  (PDHE1 $\alpha$ ), which subsequently lowered after mitotic entry (Extended Data Fig. 5f), indicative of preferential partitioning of pyruvate to lactate at the expense of mitochondrial utilization. Similarly, in synchronized mouse primary CD8 $^+$  T cells, stimulation with proliferative cytokines was sufficient to promote S-phase entry for 40% of the population by 16 h and mitotic entry for 15% of the population by 24 h (Extended Data Fig. 5g). This transition coincided with more than twofold accumulation of intracellular lactate (Extended Data Fig. 5g). Thus, proliferative cells naturally accumulate lactate to the concentrations required to remodel APC/C upon mitotic entry (Extended Data Fig. 5h).

Compared with wild-type cells, cells expressing APC4(K772/798R) generated similar levels of intracellular lactate upon mitotic entry (Fig. 4a,b and Extended Data Fig. 5c). Despite this, cells lacking these SUMOylation targets exhibited severely compromised degradation of cyclin B1 and securin, and inhibition of mitotic exit (Fig. 4a,b and Extended Data Fig. 5c). We next examined whether the accumulation of lactate upon mitotic entry was sufficient to regulate these effects on

mitosis. We applied interventions to lower the abundance of intracellular lactate. First, we engineered cells expressing lactate monooxygenase (LMO), a bacterial oxidoreductase that catalyses the oxidation of lactate in the presence of oxygen<sup>44</sup> (Extended Data Fig. 5i). LMO-dependent catabolism of intracellular lactate diminished its accumulation upon mitotic entry (Extended Data Fig. 5j), which significantly prolonged stabilization of cyclin B1 and securin during mitosis (Fig. 4c) and extended the time in mitosis (Fig. 4c,d). We also treated cells with the mitochondrial PDK inhibitor sodium dichloroacetate (DCA), which antagonizes lactate production by preferentially driving oxidation of pyruvate by mitochondria<sup>45</sup>. Treatment of cells with DCA significantly inhibited the accumulation of intracellular lactate upon mitotic entry (Extended Data Fig. 5j). DCA-induced lowering of lactate significantly prolonged the stabilization of cyclin B1 and securin during mitosis (Fig. 4c) and significantly extended time in mitosis (Fig. 4c,e).

We next explored whether lactate-dependent remodelling of APC/C composition has a role in regulating rates of cellular proliferation. We examined intracellular lactate abundance in 707 human cancer cell lines<sup>46</sup> and observed a highly significant negative correlation with doubling time (Extended Data Fig. 5k). Thus, we determined whether proliferation rates in high-lactate-producing cells were dependent on lactate-mediated stabilization of APC4–SUMO2/3. We first monitored proliferation in wild-type and APC4(K772/798R) HeLa S3 and HCT116 cells, and observed significantly diminished proliferation rates in cells lacking APC4–SUMO sites (Extended Data Fig. 5l). We also examined these effects in the presence of 1% O<sub>2</sub>, conditions in which intracellular lactate abundance is further increased, which coincides with lower abundance of cyclin B1 and securin (Extended Data Fig. 5m). Again, we observed significant diminution of proliferation rates in cells lacking APC4–SUMO sites (Extended Data Fig. 5n). Next, we determined the effects of preventing lactate accumulation, by LMO expression or DCA treatment, on proliferation rates. Lowering of intracellular lactate by either approach significantly inhibited cellular proliferation (Fig. 4f,g). These anti-proliferative effects were lost in APC4(K772/798R) cells (Fig. 4f,g), indicating that the consequences of lactate accumulation on proliferation required these SUMOylation sites.

### Lactate drives mitotic slippage

Proliferating cells exhibit oscillations in intracellular lactate levels, with high concentrations observed upon mitotic entry (Fig. 4a and Extended Data Fig. 5c). Because of the requirement for efficient exchange of intracellular lactate with extracellular fluids, physiological settings in which lactate export is compromised results in chronically increased lactate in the microenvironment<sup>47</sup>. Poorly vascularized and hypoxic tumours are prominent examples of this phenomenon, which is associated with poor prognosis<sup>47</sup>. We therefore examined whether chronically increased lactate concentrations result in aberrant regulation of APC/C and mitosis in proliferating cells (Extended Data Fig. 6a).

We first studied asynchronous HeLa S3, HCT116 and DLD1 cells, which exhibit average intracellular lactate concentrations of 2–10 mM (Extended Data Fig. 6b). Treatment of asynchronous cells with exogenous lactate at 15–25 mM was sufficient to lower levels of cyclin B1 and securin within 4 h (Extended Data Fig. 6c). Perturbations that increase endogenous lactate levels elicited similar effects to those observed following exogenous lactate addition. We overexpressed FOXK1 and FOXK2 (Extended Data Fig. 6d), two transcriptional activators of glycolytic lactate production<sup>48</sup>. Separately, we subjected cells to 1% O<sub>2</sub> for 24 h to increase the reliance on glycolytic ATP. Both interventions led to a marked decrease in cyclin B1 and securin (Extended Data Figs. 5m and 6e). This effect was not attributable to changes in nutrient status, as excess glucose did not recapitulate the effect of elevated lactate (Extended Data Fig. 6f). Instead, the lactate-mediated depletion of cell cycle regulators occurred owing to lactate-mediated remodelling of APC/C, as this effect was completely lost in APC4(K772/798R)

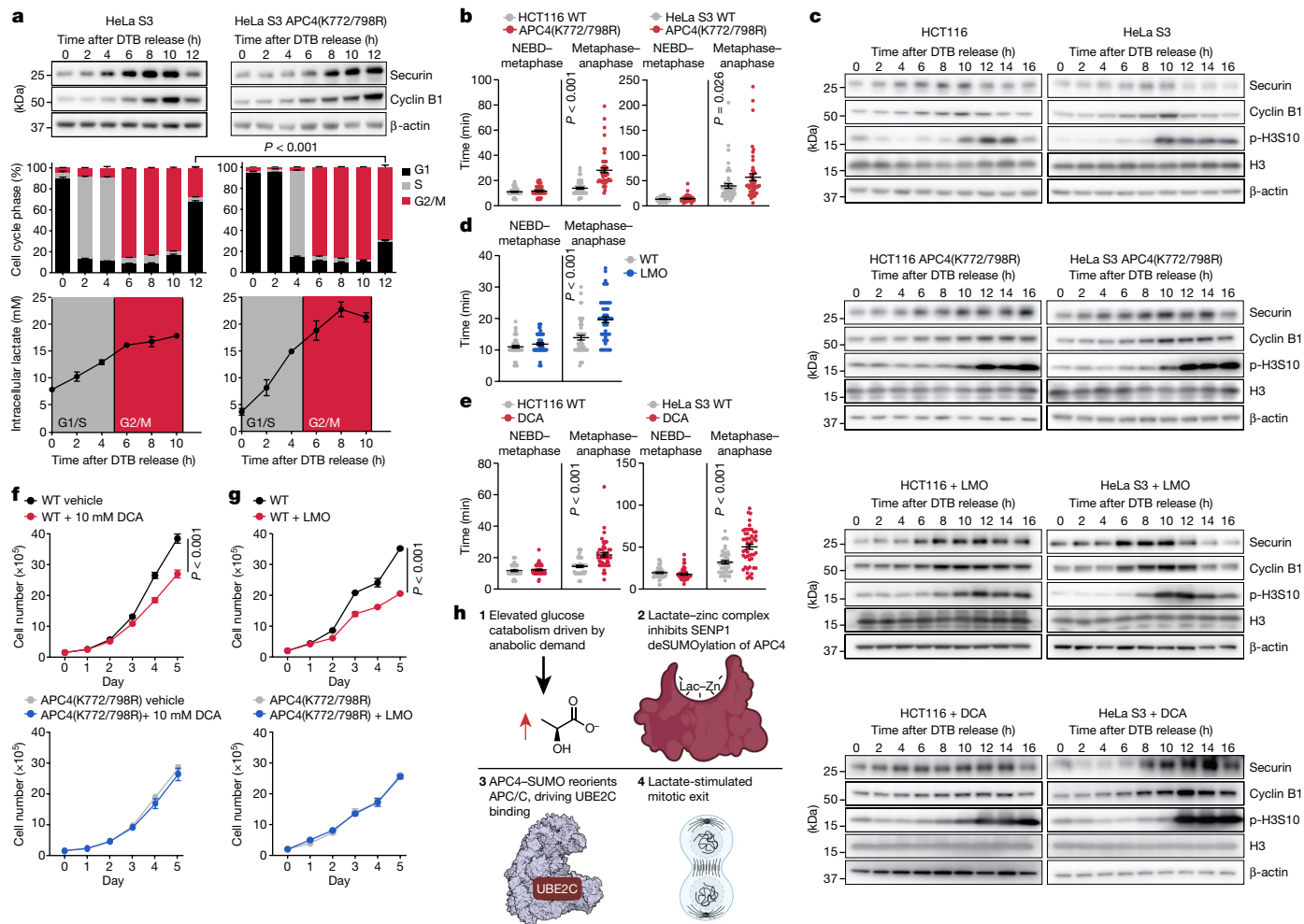


**Fig. 4 | Lactate-mediated increase in APC4-SUMO stimulates mitotic exit and proliferation.** **a**, Parallel tracking of securin and cyclin B1 abundance (top), cell cycle phase (middle) and intracellular lactate abundance (bottom) in HeLa S3 cells expressing wild-type or K772/798R APC4. Cell cycle phase: wild type,  $n = 3$ ; K772/798R,  $n = 6$  cell replicates. Lactate abundance: wild type 2 h and wild type 8 h,  $n = 5$ ; other conditions,  $n = 6$  cell replicates. Representative blot from three experiments. **b**, Mitotic progression beginning with nuclear envelope breakdown (NEBD) to metaphase plate alignment and from metaphase plate alignment to anaphase onset was quantified in wild-type and APC4(K772/798R)-expressing cells by time-lapse microscopy. HCT116: wild type,  $n = 51$ ; APC4(K772/798R),  $n = 53$  individual cell replicates. HeLa S3: wild type,  $n = 50$ ; APC4(K772/798R),  $n = 49$  individual cell replicates. **c**, Parallel tracking of securin, cyclin B1 and phosphorylated histone H3 serine 10 (p-H3S10) abundance in wild-

type, APC4(K772/798R)-expressing, LMO-expressing and 25 mM DCA-treated cells. Representative blot from three experiments. **d,e**, Mitotic progression, beginning with NEBD to metaphase plate alignment and from metaphase plate alignment to anaphase onset, was quantified in wild-type, LMO-expressing (**d**;  $n = 53$ ) and 25 mM DCA-treated cells (**e**) by time-lapse microscopy. HeLa S3,  $n = 46$ ; HeLa S3 + DCA,  $n = 49$  individual cell replicates. HCT116,  $n = 48$ ; HCT116 + DCA,  $n = 48$  individual cell replicates. **f,g**, Proliferation rate of wild-type and APC4(K772/798R)-expressing HCT116 cells treated with or without 10 mM DCA (**f**;  $n = 6$ ) or expressing LMO (**g**;  $n = 3$ ).  $n$  refers to the number of cell replicates. Two-way ANOVA for multiple comparisons involving two independent variables with Bonferroni's post hoc test. **h**, Mechanistic model of lactate regulation over the cell cycle via inhibition of SENP1. **a,b,d,e**, Two-tailed Student's *t*-test for pairwise comparisons. Data are mean  $\pm$  s.e.m.

cells (Extended Data Fig. 6g). Moreover, inhibition of the proteasome completely reversed the effect of lactate (Extended Data Fig. 6h), and these effects were independent of lactate metabolism as they persisted in the presence of an LDH inhibitor (Extended Data Fig. 6i). Next, we acutely increased cellular lactate production using the mitochondrial ATP synthase inhibitor oligomycin A to promote reliance on glycolytic ATP. Separately, we treated cells with a pan-MCT inhibitor to prevent glycolytically-derived lactate from being exported from cells<sup>9</sup>. Both interventions lowered levels of cyclin B1 and securin, and this effect required SUMOylation of APC4(K772/798) (Extended Data Fig. 6j,k).

Persistent high levels of lactate in cancers is associated with therapeutic resistance and poor prognosis<sup>49</sup>. Anti-mitotic drugs are widely used to treat cancers via disruption of microtubule assembly. Therapeutic resistance to anti-mitotic drugs is associated with mitotic slippage: a phenomenon of mitotic progression in the absence of microtubule

assembly<sup>50</sup>. Mitotic slippage depends on depletion of cyclin B1, which overcomes mitotic arrest despite an intact spindle assembly checkpoint, but the basis for this aberrant degradation is unclear<sup>50</sup>. However, it has been reported that loss of SENP1 renders cells amenable to increased mitotic slippage<sup>51</sup>. We explored the effects of increased lactate concentration in synchronized HeLa S3 and HCT116 cells arrested by nocodazole to inhibit microtubule assembly and antagonize mitotic exit. As expected, nocodazole stabilized cyclin B1 and arrested cells in pro-metaphase (Extended Data Fig. 7a). However, treatment of arrested cells with high lactate resulted in significant depletion of cyclin B1 (Extended Data Fig. 7a). Similarly, pharmacological increase of intracellular lactate with oligomycin A or a pan-MCT inhibitor drove cyclin B1 depletion (Extended Data Fig. 7b,c). Acute elevation of lactate significantly increased the rate of mitotic progression in nocodazole-arrested cells and increased the frequency of chromosome mis-segregation

(Extended Data Fig. 7d–g). Furthermore, lactate-mediated degradation of cyclin B1, mitotic rate stimulation and chromosome mis-segregation in the presence of nocodazole were abrogated in APC4(K772/798R) cells (Extended Data Fig. 7a–g). Therefore, a persistently high lactate concentration is sufficient to counteract mitotic arrest initiated by microtubule disruption, via remodelling of APC/C.

## Discussion

On the basis of our findings, we propose a mechanism of biological regulation directly controlled by accumulation of the metabolic end-product of glycolysis (Fig. 4h). We found that lactate can form an inhibitory complex with zinc in the active site of the cysteine protease SENP1. This lactate-mediated inhibition of SENP1 rapidly stabilizes SUMOylation of APC4, resulting in the reorientation of APC/C to permit UBE2C binding. Remodelling of APC/C by lactate potentiates the degradation of cyclin B1 and securin, which regulates mitotic exit. Moreover, proliferative cells accumulate lactate to thresholds required to initiate this cascade upon mitotic entry. In this way, accumulated lactate serves as an overarching signal for the degree of flux to anabolic and energetic processes tied to glycolysis during growth phase metabolism. By extension, lactate-mediated remodelling of APC/C communicates the consequences of nutrient-replete anabolism to regulate mitosis. This mechanism appears to be subject to maladaptation, as persistent elevation of lactate concentration is sufficient to drive aberrant depletion of cell cycle regulators and mitotic slippage through APC/C.

Formation of a complex with zinc in SENP1 could generalize to other biological settings where substantial quantities of lactate are produced in the absence of proliferation, including, for example, in adipocyte hypertrophy and exercising muscle. On this basis, a clear priority for future research will be to identify the breadth of SENP1 targets regulated by lactate, an interaction that could serve as a general metabolic signal of increased glycolysis in many biological settings.

## Online content

Any methods, additional references, Nature Portfolio reporting summaries, source data, extended data, supplementary information, acknowledgements, peer review information; details of author contributions and competing interests; and statements of data and code availability are available at <https://doi.org/10.1038/s41586-023-05939-3>.

1. Warburg, O. On the origin of cancer cells. *Science* **123**, 309–314 (1956).
2. Koppenol, W. H., Bounds, P. L. & Dang, C. V. Otto Warburg's contributions to current concepts of cancer metabolism. *Nat. Rev. Cancer* **11**, 325–337 (2011).
3. Wang, T., Marquardt, C. & Foker, J. Aerobic glycolysis during lymphocyte proliferation. *Nature* **261**, 702–705 (1976).
4. Brand, K., Leibold, W., Luppa, P., Schoerner, C. & Schulz, A. Metabolic alterations associated with proliferation of mitogen-activated lymphocytes and of lymphoblastoid cell lines: evaluation of glucose and glutamine metabolism. *Immunobiology* **173**, 23–34 (1986).
5. Munyon, W. H. & Merchant, D. J. The relation between glucose utilization, lactic acid production and utilization and the growth cycle of L strain fibroblasts. *Exp. Cell. Res.* **17**, 490–498 (1959).
6. Lemaigne, M., Aubert, J. P. & Millet, J. Ethyl alcohol production and growth of baker's yeast cultured under aerobic conditions. *Ann. Inst. Pasteur* **87**, 427–439 (1954).
7. Luengo, A. et al. Increased demand for NAD<sup>+</sup> relative to ATP drives aerobic glycolysis. *Mol. Cell* **81**, 691–707.e696 (2021).
8. Dai, Z., Shestov, A. A., Lai, L. & Locasale, J. W. A flux balance of glucose metabolism clarifies the requirements of the Warburg effect. *Biophys. J.* **111**, 1088–1100 (2016).
9. Halestrap, A. P. The monocarboxylate transporter family—Structure and functional characterization. *IUBMB Life* **64**, 1–9 (2012).
10. Hui, S. et al. Glucose feeds the TCA cycle via circulating lactate. *Nature* **551**, 115–118 (2017).
11. Faubert, B. et al. Lactate metabolism in human lung tumors. *Cell* **171**, 358–371.e359 (2017).
12. Walenta, S. et al. High lactate levels predict likelihood of metastases, tumor recurrence, and restricted patient survival in human cervical cancers. *Cancer Res.* **60**, 916–921 (2000).
13. Walenta, S. et al. Tissue gradients of energy metabolites mirror oxygen tension gradients in a rat mammary carcinoma model. *Int. J. Radiat. Oncol. Biol. Phys.* **51**, 840–848 (2001).
14. Quinn, W. J. 3rd et al. Lactate limits T cell proliferation via the NAD(H) redox state. *Cell Rep.* **33**, 108500 (2020).
15. Mateus, A. et al. Thermal proteome profiling for interrogating protein interactions. *Mol. Syst. Biol.* **16**, e9232 (2020).
16. Jin, L., Williamson, A., Banerjee, S., Philipp, I. & Rape, M. Mechanism of ubiquitin-chain formation by the human anaphase-promoting complex. *Cell* **133**, 653–665 (2008).
17. Reddy, S. K., Rape, M., Margansky, W. A. & Kirschner, M. W. Ubiquitination by the anaphase-promoting complex drives spindle checkpoint inactivation. *Nature* **446**, 921–925 (2007).
18. Sivakumar, S. & Gorsky, G. J. Spatiotemporal regulation of the anaphase-promoting complex in mitosis. *Nat. Rev. Mol. Cell Biol.* **16**, 82–94 (2015).
19. Yamaguchi, M. et al. Cryo-EM of mitotic checkpoint complex-bound APC/C reveals reciprocal and conformational regulation of ubiquitin ligation. *Mol. Cell* **63**, 593–607 (2016).
20. Chang, L., Zhang, Z., Yang, J., McLaughlin, S. H. & Barford, D. Atomic structure of the APC/C and its mechanism of protein ubiquitination. *Nature* **522**, 450–454 (2015).
21. Brown, N. G. et al. RING E3 mechanism for ubiquitin ligation to a disordered substrate visualized for human anaphase-promoting complex. *Proc. Natl. Acad. Sci. USA* **112**, 5272–5279 (2015).
22. Savitski, M. M. et al. Tracking cancer drugs in living cells by thermal profiling of the proteome. *Science* **346**, 1255784 (2014).
23. Watson, E. R., Brown, N. G., Peters, J. M., Stark, H. & Schulman, B. A. Posing the APC/C E3 ubiquitin ligase to orchestrate cell division. *Trends Cell Biol.* **29**, 117–134 (2019).
24. Alfieri, C. et al. Molecular basis of APC/C regulation by the spindle assembly checkpoint. *Nature* **536**, 431–436 (2016).
25. Brown, N. R. et al. CDK1 structures reveal conserved and unique features of the essential cell cycle CDK. *Nat. Commun.* **6**, 6769 (2015).
26. Brown, N. R. et al. Cyclin B and cyclin A confer different substrate recognition properties on CDK2. *Cell Cycle* **6**, 1350–1359 (2007).
27. Flotho, A. & Melchior, F. Sumoylation: a regulatory protein modification in health and disease. *Annu. Rev. Biochem.* **82**, 357–385 (2013).
28. Lee, C. C., Li, B., Yu, H. & Matunis, M. J. Sumoylation promotes optimal APC/C activation and timely anaphase. *eLife* **7**, e29539 (2018).
29. Eifler, K. et al. SUMO targets the APC/C to regulate transition from metaphase to anaphase. *Nat. Commun.* **9**, 1119 (2018).
30. Yatskevich, S. et al. Molecular mechanisms of APC/C release from spindle assembly checkpoint inhibition by APC/C SUMOylation. *Cell Rep.* **34**, 108929 (2021).
31. Mukhopadhyay, D. & Dasso, M. Modification in reverse: the SUMO proteases. *Trends Biochem. Sci.* **32**, 286–295 (2007).
32. Cubenas-Potts, C., Goeres, J. D. & Matunis, M. J. SENP1 and SENP2 affect spatial and temporal control of sumoylation in mitosis. *Mol. Biol. Cell* **24**, 3483–3495 (2013).
33. Ireland, S. M. & Martin, A. C. R. ZincBind—the database of zinc binding sites. *Database* **2019**, baz006 (2019).
34. Skiles, J. W., Gonnella, N. C. & Jeng, A. Y. The design, structure, and therapeutic application of matrix metalloproteinase inhibitors. *Curr. Med. Chem.* **8**, 425–474 (2001).
35. Jacobsen, J. A., Major Jourden, J. L., Miller, M. T. & Cohen, S. M. To bind zinc or not to bind zinc: an examination of innovative approaches to improved metalloproteinase inhibition. *Biochim. Biophys. Acta* **1803**, 72–94 (2010).
36. Cannan, R. K. & Kibrick, A. Complex formation between carboxylic acids and divalent metal cations. *J. Am. Chem. Soc.* **60**, 2314–2320 (1938).
37. Thun, H., Guns, W. & Verbeek, F. The stability constants of some bivalent metal complexes of α-hydroxyisobutyrate and lactate. *Anal. Chim. Acta* **37**, 332–338 (1967).
38. Pace, N. J. & Weerapana, E. A competitive chemical-proteomic platform to identify zinc-binding cysteines. *ACS Chem. Biol.* **9**, 258–265 (2014).
39. Hann, M. M. & Simpson, G. L. Intracellular drug concentration and disposition—the missing link. *Methods* **68**, 283–285 (2014).
40. Schwaid, A. G. & Cornella-Taracido, I. Causes and significance of increased compound potency in cellular or physiological contexts. *J. Med. Chem.* **61**, 1767–1773 (2018).
41. Swinney, D. C. Biochemical mechanisms of drug action: what does it take for success. *Nat. Rev. Drug Discov.* **3**, 801–808 (2004).
42. Fasano, M. et al. The extraordinary ligand binding properties of human serum albumin. *IUBMB Life* **57**, 787–796 (2005).
43. Colombo, S. L. et al. Molecular basis for the differential use of glucose and glutamine in cell proliferation as revealed by synchronized HeLa cells. *Proc. Natl. Acad. Sci. USA* **108**, 21069 (2011).
44. Maeda-Yorita, K., Aki, K., Sagai, H., Misaki, H. & Massey, V. L-lactate oxidase and L-lactate monoxygenase: mechanistic variations on a common structural theme. *Biochimie* **77**, 631–642 (1995).
45. Stacpoole, P. W., Nagaraja, N. V. & Hutson, A. D. Efficacy of dichloroacetate as a lactate-lowering drug. *J. Clin. Pharmacol.* **43**, 683–691 (2003).
46. Li, H. et al. The landscape of cancer cell line metabolism. *Nat. Med.* **25**, 850–860 (2019).
47. Parks, S. K., Mueller-Klieser, W. & Pouysségur, J. Lactate and acidity in the cancer microenvironment. *Annu. Rev. Cancer Biol.* **4**, 141–158 (2020).
48. Sukonika, V. et al. FOXK1 and FOXK2 regulate aerobic glycolysis. *Nature* **566**, 279–283 (2019).
49. Parks, S. K., Chiche, J. & Pouysségur, J. Disrupting proton dynamics and energy metabolism for cancer therapy. *Nat. Rev. Cancer* **13**, 611–623 (2013).
50. Lens, S. M. A. & Medema, R. H. Cytokinesis defects and cancer. *Nat. Rev. Cancer* **19**, 32–45 (2019).
51. Era, S. et al. The SUMO protease SENP1 is required for cohesion maintenance and mitotic arrest following spindle poison treatment. *Biochem. Biophys. Res. Commun.* **426**, 310–316 (2012).

**Publisher's note** Springer Nature remains neutral with regard to jurisdictional claims in published maps and institutional affiliations.

Springer Nature or its licensor (e.g. a society or other partner) holds exclusive rights to this article under a publishing agreement with the author(s) or other rightsholder(s); author self-archiving of the accepted manuscript version of this article is solely governed by the terms of such publishing agreement and applicable law.

© The Author(s), under exclusive licence to Springer Nature Limited 2023

## Methods

### Thermal proteomic profiling

HEK 293 cells were grown in 12×15-cm dishes (4×15-cm dishes per group). Cells were washed twice with ice-cold PBS. Cells were then gently scraped in 5 ml per dish of PBS, transferred into 15-ml conical tubes and centrifuged at 1,000g for 3 min at 4 °C to pellet cells. Supernatant was carefully removed, then 1 ml per tube of PBS containing 0.5% IGEPAL (v/v) supplemented with protease inhibitors was added. Two pellets were combined into a tube and were homogenized and centrifuged at 1,900g for 10 min. The supernatants were combined into a fresh 50-ml conical tube. Zeba Spin Desalting Columns (Thermo Scientific) were used for buffer exchange into 5 ml PBS + 0.5% IGEPAL. Protein concentration was determined by using the bicinchoninic acid (BCA) assay (Pierce), and protein concentration was adjusted to 1 mg ml<sup>-1</sup>. Then, 1.75 ml per tube of protein samples was added into 3×2-ml tubes. Protein samples were treated for 15 min with different concentrations of sodium lactate or sodium chloride with mild agitation at room temperature. Each cell suspension with vehicle control or with lactate was distributed into 10×0.2-ml PCR tubes (150 µl of cell suspension per tube). The PCR-tube strips were heated at their designated temperature for 3 min in a Veriti 96-well thermal cycler. Then the samples were centrifuged at max speed for 1.5 h at 4 °C. For western blotting, 60 µl of the supernatant was transferred to a 1.5-ml tube, mixed with 20 µl of 4×NuPAGE LDS sample buffer (Invitrogen, NP0007) supplemented with 10% 2-mercaptoethanol and boiled at 95 °C for 10 min. For proteomics experiments, 60 µl of the supernatant was transferred to a 1.5-ml tube containing 50 µl of lysis buffer (2% SDS, 150 mM NaCl, 50 mM HEPES pH 8.8, 50 µM TCEP, protease inhibitor, HPLC water). Samples were reduced at 60 °C for 30 min. Then the samples were brought back to room temperature and centrifuged at 500g for 5 min. Iodoacetamide was added (final concentration 14 mM) and samples were incubated in dark for 45 min. Then dithiothreitol was added (final concentration 5 mM) and samples were incubated in dark for 15 min. After incubation, 30 µl of 100% TCA was added and samples were vortexed briefly and incubated at 4 °C on ice overnight.

### Protein digestion and TMT labelling

Protein pellets were dried and resuspended in 8 M urea containing 50 mM HEPES (pH 8.5). Protein concentrations were measured by BCA assay (Thermo Scientific) before protease digestion. Protein lysates were diluted to 4 M urea and digested with LysC (Wako, Japan) in a 1/100 enzyme/protein ratio overnight. Protein extracts were diluted further to a 1.0 M urea concentration, and trypsin (Promega) was added to a final 1/200 enzyme/protein ratio for 6 h at 37 °C. Digests were acidified with 20 µl of 20% formic acid to a pH ~2, and subjected to C18 solid-phase extraction (50 mg Sep-Pak, Waters). Peptides were then dissolved with 75 µl 200 mM EPPS and 10 µl of TMT label (8 µg per µl) was added and incubated for 30 min, followed by addition of 10 µl of TMT label and incubation for a further 30 min. The labelling reactions were quenched with 4 µl hydroxylamine (5%) solution, incubated for a further 15 min and pooled together and vacuum dried for liquid chromatography–mass spectrometry (LC–MS/MS) analysis. For TPP experiments, under each condition, samples from ten different temperatures were labelled with ten different TMT tags and pooled together as a single TMT experiment.

### LC–MS/MS parameters

An Orbitrap Eclipse Tribrid Mass Spectrometer (Thermo) coupled with an Easy-nLC1200 (Thermo) was used for proteomics measurements. A 55-min gradient consisting of 2%–30% acetonitrile (ACN), 0.125% formic acid at 500 nl/min flow rate was used to separate and analyse peptides. A FAIMSPro (Thermo) device was operated under –40V/–60V/–80V for field asymmetric waveform ion mobility spectrometry (FAIMS) separation of precursors for IP–MS experiments<sup>52</sup>.

Under each voltage, data-dependent acquisition was used mode using a mass range of *m/z* 400–1,400 using a top10 method. Resolution for MS1 was set at 120,000. Singly-charged ions were not further sequenced, and multiply-charged ions were selected and subjected to fragmentation with standard automatic gain control and 35% normalized collisional energy (NCE) for MS2, with a dynamic exclusion window of 30 s. Quantification of TMT reporter ion were performed using the multinoth SPS-MS3 method<sup>53</sup> with 45% NCE for MS3. Raw files were first converted to mzXML, and searched using the Comet algorithm<sup>54</sup> on an in-house database search engine reported previously<sup>55</sup>. Database searching included all human (*Homo sapiens*) entries from UniProt (<http://www.uniprot.org>, downloaded 2020) and the reversed sequences as well as common contaminants (such as keratins or trypsin). Peptides were searched using the following parameters: 25 ppm precursor mass tolerance; 1.0 Da product ion mass tolerance; fully tryptic digestion; up to three missed cleavages; variable modification: oxidation of methionine (+15.9949); static modifications: TMTpro (+304.2071) on lysine and peptide N terminus, carboxyamidomethylation (+57.0214637236) on cysteines. The experiment was also searched with the parameters described above with an additional variable phosphorylation (+79.966 Da) on serine, threonine, or tyrosine was added. The false discovery rate (FDR) was controlled as described previously<sup>55–57</sup> to <1% on peptide level for each mass spectrometry run using parameters such as XCorr, ΔCn, missed cleavages, peptide length, charge state and precursor mass accuracy. Then protein-level FDR was also controlled to <1%. Phosphorylation site localization was determined using the ModScore algorithm<sup>58</sup> where a score of 13 corresponds to 95% confidence in correct localization. TMT reporter ions were used for quantification of peptide abundance. Isotopic impurities were corrected according to the manufacturer's specifications, and signal-to-noise ratio (S/N) was calculated. Peptides with summed S/N lower than 160 across 16 channels of each TMTpro16 plex or isolation specificity lower than 0.5 were discarded. The high confidence peptides were then used to quantify protein abundance by summing up S/N values for all peptides assigned to the same protein, and only proteins in the linear quantification range of the instrument were included in the analysis. For IP–MS experiments, normalization for protein quantification was then performed by adjusting protein loadings to that every TMT channel has the same loading of CDC27, which is the target protein for pulldown.

### Data processing for TPP

For reporter ion quantification, a 0.003 Da window around the theoretical *m/z* of each reporter ion was scanned, and the most intense *m/z* was used. Reporter ion intensities were adjusted to correct for the isotopic impurities of the different TMT reagents according to manufacturer specifications. Peptides were filtered to include only those with a summed S/N of 200 or greater across all channels. An isolation purity of at least 0.7 in the MS1 isolation window was used. Temperature cure plex strategy followed published approaches<sup>59,60</sup>. For each protein, the filtered peptide TMT S/N values were summed to generate protein quantification. Within each 10-plex, protein abundance at every temperature was normalized to abundance at 37 °C. To compare changes in thermostability between conditions, normalized temperature curves were compared. In lactate-treated conditions, normalized abundance of every protein, at each temperature, was compared to the normalized abundance of the same protein in the NaCl control. Then, for each protein an integrated stabilization value was generated by summing the difference in normalized abundance at every temperature. The entire proteome was then assessed in terms of change in stabilization, comparing 15 mM lactate and 25 mM lactate, to control.

### Mass spectrometry identification of lysine lactylation

Searches were conducted using the Comet algorithm<sup>54</sup> on an in-house database search engine reported previously<sup>55</sup>. Database searching

included all human entries from UniProt (<http://www.uniprot.org>, downloaded on 24 November 2021) appended with reversed sequences and common contaminants. Peptides were searched using the following parameters: 25 ppm precursor mass tolerance; 1.0 Da product ion mass tolerance; fully tryptic digestion; up to three missed cleavages; variable modification: oxidation of methionine (+15.9949), lysine lactoylation (-232.1861, which is the mass difference between TMTpro +304.2071 and lactoylation +72.021); static modifications: TMTpro (+304.2071) on lysine and peptide N terminus, carboxyamidomethylation (+57.0214637236) on cysteines. The target-decoy method was used to control the FDR<sup>55–57</sup> to <1% on peptide level. Peptides that are shorter than seven amino acids were discarded.

### Cell synchronization

For thymidine–nocodazole block to obtain populations of cells in pro-metaphase, cells were arrested in 2 mM thymidine (Sigma, T1895) for 18–20 h, released for 4 h and blocked in 100 ng ml<sup>-1</sup> nocodazole (Sigma, M1404) for 12–14 h. For double thymidine block, cells were arrested at G1/S boundary by a double thymidine block as has previously been described<sup>61,62</sup>. In brief, cells were blocked with 2 mM thymidine for 18 h, released from the arrest for 9 h and arrested a second time with 2 mM thymidine for 18 h. After synchronization, the cells were collected or released depending on the experiment.

### Native cellular lysate incubations

Lysates from thymidine–nocodazole synchronized cells were used for IP–MS, immunoprecipitation binding and immunoprecipitation SUMO2/3 experiments. Mixture containing cell lysates, swelling buffer, 1× E-mix (7.5 mM creatine phosphate, 1 mM ATP, 1 mM MgCl<sub>2</sub>), different concentrations of sodium chloride (Fisher, S271-1), sodium lactate (Sigma, L7022) or zinc sulfate heptahydrate (Sigma, Z0251) were co-incubated in 1.5-ml tubes for 15 min prior to immunoprecipitation at 4 °C overnight, followed by downstream experiments.

### Intact cell incubations

HCT116, DLD1 and HeLa S3 cells were seeded at a density of 400,000 cells per well, 24 h prior to use. Cells were collected after incubation with different concentrations of sodium lactate (Sigma, L7022), lactic acid (Sigma, L1750), sodium D-lactate (Sigma, 71716), sodium pyruvate (Sigma, P2256) for 4 h, followed by downstream experiments.

### Cell lysate preparation for IP–MS, immunoprecipitation binding and immunoprecipitation SUMO2/3 experiments

Cells were synchronized with thymidine–nocodazole and then collected. Cell pellets were fully resuspended with ice-cold swelling buffer (20 mM HEPES pH 7.5, 5 mM KCl, 1.5 mM MgCl<sub>2</sub>, 1 mM dithiothreitol, 1× EDTA-free protease inhibitor) and E-mix (375 mM creatine phosphate, 50 mM ATP, 50 mM MgCl<sub>2</sub>). The volume of swelling buffer was 75% volume of cell pellet. The volume of E-mix was 2% volume of cell pellet plus swelling buffer. The cell lysates were incubated on ice for 30 min and flipped occasionally. After incubation, the lysates were frozen rapidly in liquid nitrogen and then thawed rapidly at 30 °C twice. After the second thawing, the lysates were sheared with a 20.5 G needle for 10 times on ice followed by centrifuge at 5,000 rpm for 5 min at 4 °C. The supernatant was collected and centrifuged again at 14,000 rpm for 60 min at 4 °C. Then the supernatant was used for following experiments.

### Immunoprecipitation of APC/C

To detect the binding between UBE2C, APC/C and its substrates, APC/C complex was immunoprecipitated from mitotic cell lysates overnight at 4 °C with the anti-CDC27 (AF3.1) antibody (Santa Cruz, sc-9972; 2 µg of antibody per sample) that was coated on protein G magnetic beads (Invitrogen, 10007D) in the presence or absence of 10 µM recombinant UBE2C. The precipitated protein was eluted in 2× NuPAGE LDS sample buffer supplemented with 10% 2-mercaptoethanol and boiled at 95 °C

for 10 min. Input samples and flow through samples were mixed with 4× NuPAGE LDS sample buffer supplemented with 10% 2-mercaptoethanol and boiled at 95 °C for 10 min. To detect SUMOylation of APC4, APC/C complex or APC4 protein was immunoprecipitated from cell lysates overnight at 4 °C with anti-CDC27 (AF3.1) antibody (Santa Cruz, sc-9972; 2 µg of antibody per sample) or anti-APC4 antibody (Bethyl Laboratories, A301-176A; 1 µg of antibody per sample), respectively. The precipitated protein was eluted in 2× NuPAGE LDS sample buffer supplemented with 10% 2-mercaptoethanol and boiled at 95 °C for 10 min, followed by western blotting.

### Immunoprecipitation of UBE2C

To detect the binding between UBE2C and APC4, UBE2C was immunoprecipitated from mitotic cell lysates overnight at 4 °C with the UBE2C antibody (Abcam, ab252940; 2 µg of antibody per sample) that was coated on protein G magnetic beads (Invitrogen 10007D) in the absence of recombinant UBE2C. The precipitated protein was eluted in 2× NuPAGE LDS sample buffer supplemented with 10% 2-mercaptoethanol and boiled at 95 °C for 10 min. Input samples and flow through samples were mixed with 4× NuPAGE LDS sample buffer supplemented with 10% 2-mercaptoethanol and boiled at 95 °C for 10 min, followed by western blotting.

### Generation of SENP1-knockout cell lines

To generate the endogenous SENP1-knockout cell lines, we designed single guide RNA (sgRNA) oligonucleotide sequences as follows: Fwd: CACCGCCATCCGCTTCCGGAAGTA; Rev: AAACTACTTCGGAAAGCG GATGCC. We used the following sgRNA oligonucleotide sequences to generate the negative control cell lines: Fwd: CACCGTCGAAATGTC CGTTCGGT; Rev: AAACACCAGACGGACATTGAAAC<sup>63</sup>. Fwd and Rev oligonucleotides were annealed and ligated into PX458 vector, which was digested by BbsI-HF restriction enzymes (NEB, R3539S). PX458 was a gift from F. Zhang (Addgene, plasmid 48138). Then, PX458 vector containing SENP1 sgRNA sequence was transfected into HeLa S3, HCT116 and DLD1 cells with Lipofectamine 3000 (Invitrogen, L3000001). Using green fluorescent protein (GFP) as fluorochrome selection tag, cells were sorted by flow cytometry 48 h post-transfection. After 3 weeks, the isolated cell colony was validated for SENP1 expression by immunoblot analysis.

### Generation of APC4 mutant cell lines

To generate the endogenous APC4-knockout cell line, we designed sgRNA oligonucleotide sequences as follows: Fwd: CACCGATGA GTCTTCAGATGAAG; Rev: AAACCTTCATCTGAAGACTCATCC; Fwd and Rev oligonucleotides were annealed and ligated into pX458 vector, digested by BbsI-HF restriction enzymes. Then, pX458 vector containing APC4 sgRNA sequences was transfected into HeLa S3 or HCT116 cells with Lipofectamine 3000. Using GFP as a fluorochrome selection tag, cells were sorted by flow cytometry 48 h post-transfection. After 3 weeks, the isolated cell colony was validated for APC4 sequence, and APC4 expression by immunoblot analysis. The ANAPC4 expression plasmid was purchased from ORIGENE (RC209242L4). To obtain APC4 wild-type plasmid which expresses APC4 protein without mGFP-tag in C-terminal, we inserted TAA sequence at the end of ANAPC4 ORF region in the purchased plasmid using PCR-based Mut Express II Fast Mutagenesis kit (Vazyme, C214). Then, APC4 double mutant (DM) plasmid (APC4 K772/798R) was generated using APC4 wild-type plasmid as template. Lenti-X 293T, HeLa S3 and HCT116 cells were used to generate stable cell lines. Firstly, 12 µg of APC4 WT/DM plasmid, 9 µg of psPAX2 (a gift from D. Trono, Addgene, 12260), 4.5 µg of pMD2.G (a gift from D. Trono, Addgene, 12259) were co-transfected into lenti-X 293T cells with Lipofectamine 3000 according to the manufacturer's instructions. The viral supernatant was filtered through a 0.45-µm PES filter 48 h post-transfection and then infected APC4-knockout cell lines (HeLa S3 and HCT116) in the presence of 8 µg ml<sup>-1</sup> Polybrene. Medium change was done 24 h post-infection. After incubated in complete medium for 24 h,

# Article

cells were selected with puromycin ( $1\text{ }\mu\text{g ml}^{-1}$  for HeLa S3 and  $2\text{ }\mu\text{g ml}^{-1}$  for HCT116). After one week, cells were validated for APC4 expression and SUMOylation by immunoblot and immunoprecipitation analysis.

## Generation of FOXK1- and FOXK2-over-expressing cell lines

We designed CRISPRa sgRNA oligonucleotide sequences for FOXK1 over-expressing cells as follows: sgRNA1, Fwd: CACCGGCCGGCGCG ATCTGGCC; Rev: AAACGGGCCAGATCGCCGGCG; sgRNA2, Fwd: CACCGGGCGAGGCGAGGCGCACGGT; Rev: AAACACCGTGCACCC TCGCCTCGCC. We used the following CRISPRa sgRNA oligonucleotide sequences to generate FOXK2-over-expressing cell lines: sgRNA1, Fwd: CACCGACGGTTACGCCGGCAATGG; Rev: AAACCCATTGGCCGG CGTAACCGT; sgRNA2, Fwd: CACCGGACACGTGCGACCAAGCTGC, Rev: AAACCGCAGCTTGGTGCACGGTGC. Fwd and Rev oligonucleotides were annealed and cloned into LentiSAM vector (a gift from F. Zhang, Addgene, 75112) using NEB Golden Gate Assembly premade mix (NEB, E1602). Then LentiSAM contained *FOXK1* or *FOXK2* sgRNA oligos and LentiMPHv2 (a gift from F. Zhang, Addgene, 89308) were packaged by Lenti-X Packaging Single Shots (VSV-G) (Takara, 631275) and Lenti-X 293T cells, respectively. The viral supernatant was filtered through a  $0.45\text{-}\mu\text{m}$  PES filter 48 h post-transfection. First, HCT116 cells were infected with the packaged LentiSAMv2 viral supernatants in the presence of  $8\text{ }\mu\text{g ml}^{-1}$  Polybrene. Medium change was done 24 h post-infection. After incubation in complete medium for 24 h, cells were selected with  $20\text{ }\mu\text{g ml}^{-1}$  blasticidin. After 1 week, cells were infected again with the packaged LentiMPHv2 viral supernatants and then selected with  $800\text{ }\mu\text{g ml}^{-1}$  hygromycin. Cells were validated for *FOXK1* and *FOXK2* expression by quantitative PCR (qPCR) after selection for one week.

## Generation of LMO-expressing cell lines

We shuttled LMO coding cassettes from pCMV-LMO-IRES-EGFP, a gift from A. Teschemacher, to pLenti CMV GFP Puro (658-5) vector (a gift from E. Campeau and P. Kaufman, Addgene, 17448). Lenti-X 293T, APC4 wild-type and K772/798R cell lines (HeLa S3 and HCT116) were used to generate stable cell lines. First,  $9.5\text{ }\mu\text{g}$  of pLenti CMV GFP Puro (658-5),  $9\text{ }\mu\text{g}$  of psPAX2,  $4.5\text{ }\mu\text{g}$  of pMD2.G were co-transfected into Lenti-X 293T cells with Lipofectamine 3000 according to manufacturer's instructions. The viral supernatant was filtered through a  $0.45\text{-}\mu\text{m}$  PES filter 48 h post-transfection and then infected APC4 wild-type and K772/798R cell lines (HeLa S3 and HCT116) in the presence of  $8\text{ }\mu\text{g ml}^{-1}$  Polybrene. Medium change was done 24 h post-infection. Using GFP as fluorochrome selection tag, cells were sorted by flow cytometry after incubation in complete medium for 3 days.

## Generation of H2B-mCherry-expressing cell lines

pLenti.PGK.H2B-chFP.W plasmid (a gift from R. Lansford, Addgene, 51007) was used to generate H2B-mCherry stable cell lines. Firstly,  $9.5\text{ }\mu\text{g}$  of pLenti.PGK.H2B-chFP.W,  $9\text{ }\mu\text{g}$  of psPAX2,  $4.5\text{ }\mu\text{g}$  of pMD2.G were co-transfected into Lenti-X 293T cells with Lipofectamine 3000 according to manufacturer's instructions. The viral supernatant was filtered through a  $0.45\text{-}\mu\text{m}$  PES filter 48 h post-transfection and then infected APC4 wild-type, K772/798R and knockout cell lines (HeLa S3 and HCT116) and HCT116 LMO-expressing cell line in the presence of  $8\text{ }\mu\text{g ml}^{-1}$  Polybrene. Medium change was done 24 h post-infection. After incubation in complete medium for 3 days, cells were sorted by flow cytometry using mCherry as fluorochrome selection tag.

## Maintenance of cell lines

All cell lines were grown in DMEM (Corning, 10-017-CV) without pyruvate, supplemented with 10% FBS (GeminiBio, 100-106) and 1% penicillin/streptomycin (Corning, 30-002-CI). Cells were detached using 0.25% trypsin (Gibco, 25200-056) and subcultured every other day. All experiments were performed with HCT116, HeLa S3, HEK 293 and DLD1 cells obtained from ATCC.

## Measurement of intracellular volume

For each experiment examining intracellular lactate abundance, a replicate set of cells was treated identically and used for measuring volume, as described before<sup>64,65</sup>. In brief, cells were brought to suspension by incubation with trypsin for 5 min. Next, the cell number and volume were measured by using a Beckman Z2 Coulter Counter with a size setting adjusted according to cell type. Whole-cell metabolite concentrations were calculated using the total moles of a metabolite in a whole-cell sample, the total number of cells per sample, and the volume of each cell.

## Exposure to hypoxia

Cells were seeded at a density of 80,000 cells per well, 24 h prior to use. Cell culture medium (DMEM supplemented with 10% FBS and 1% penicillin/streptomycin) was placed in a sealed hypoxic chamber set to 1% oxygen tension, 24 h prior to use. On the day of the experiment, cells were placed in the hypoxic chamber for 24 h and previously degassed medium was added to each well. After the 24 h, cells were collected for downstream analysis.

## Time-lapse microscopy

Cells were seeded at a density of 200,000 cells per well in a 6-well plate, 24 h prior to use. To analyse mitotic delay or mitotic defects, APC4 wild-type, K772/798R or knockout cells (HeLa S3 and HCT116) and HCT116 LMO-expressing cells, which stably expressed H2B-mCherry, were imaged by BioTek Cytation 5 image system. For the experiments involving DCA treatment, cells were treated with 25 mM NaCl or DCA for 6 h before imaging. Time from NEBD to metaphase plate alignment and from metaphase plate alignment to anaphase onset were quantified<sup>28</sup>. Abnormal mitosis was defined as presence of lagging chromosomes, chromosomes bridge, anaphase occurring in the presence of unaligned chromosomes (as indicated by chromosomes segregation without the formation of a metaphase plate), an inability to maintain a metaphase plate (as indicated by chromosomes that keep shifting between aligned stage and unaligned stage for one or more cycles before anaphase), cell death (as indicated by cytoplasmic blebbing and irregular shapes of cells), and division into three cells. The percentage of abnormal mitotic events was determined as the number of cells with one or more kinds of abnormal mitosis divided by the total number of cells undergoing mitosis. To analyse mitotic checkpoint override or chromosome mis-segregation, APC4 wild-type or K772/798R cells (HeLa S3 and HCT116) were arrested in pro-metaphase by 2 mM thymidine and 100 ng ml<sup>-1</sup> nocodazole treatment as described above. Imaging was initiated at the beginning of nocodazole and 25 mM NaCl or sodium lactate treatment. Duration of mitotic arrest was defined as the time from NEBD until DNA decondensation. Chromosome mis-segregation includes one or more lagging chromosomes, asymmetric segregation and multipolar segregation of chromosomes. Phase-contrast and fluorescence images were captured at 5-min intervals for 18–24 h. All imaging experiments were manually analysed with Gen5 3.10 software.

## Isolation and culture of T cells

CD8a<sup>+</sup> T cells were isolated from the spleens and lymph nodes (knees, elbow, underarm and head) of C57BL/6 mice using the EasySep Mouse CD8a positive selection kit II (Stem Cell Technologies, 18953) (PMC6237851). Purified mouse CD8a<sup>+</sup> T cells were resuspended in T cell medium (RPMI-1640, 10% fetal calf serum, 1% glutamine and 14.2 mM  $\beta$ -mercaptoethanol) containing IL-2 (10 ng ml<sup>-1</sup>) and anti-CD28 (0.5  $\mu\text{g ml}^{-1}$ ). Cells were plated in well pre-coated with anti-CD3 (5  $\mu\text{g ml}^{-1}$ ) coated plates at a density of  $\sim 2 \times 10^6$  cells per ml.

## Western blotting

Samples were isolated in RIPA buffer (50 mM Tris, pH 7.4, 150 mM NaCl, 1% Triton X-100, 0.5% sodium deoxycholate, 0.1% SDS, 1 mM EDTA)

supplemented with a cocktail of protease inhibitors (Roche). Cell lysates were centrifuged at 14,000 rpm for 15 min at 4 °C, and the supernatants were used for subsequent analysis. Protein concentration was determined using the bicinchoninic acid (BCA) assay (Pierce). Protein lysates were mixed with NuPAGE LDS sample buffer (Invitrogen, NP0007) supplemented with 10% 2-mercaptoethanol and boiled at 95 °C for 10 min. Samples were resolved by 4–12% NuPAGE Bis-Tris protein gels (Invitrogen, NP0336) and transferred to a polyvinylidene difluoride (PVDF) membrane (Millipore). Primary antibodies (UBE2C (Abcam, ab252940; 1:1,000); cyclin B1 (CST, 12231; 1:1,000); Securin (CST, 13445; 1:1,000); SUMO2/3 (Abcam, ab81371; 1:1,000); SUMO1 (PTM BIO, PTM-6055; 1:500); SENP1 (Proteintech, 25349-1-AP; 1:1,000); CDC27 (Santa Cruz, sc-9972; 1:1,000); APC4 (Bethyl Laboratories, A301-176A; 1:1,000); H3 (CST, 4499; 1:1,000); phos-H3S10 (CST, 53348; 1:1,000), PDH (CST, 3205; 1:1,000); phos-PDH(CST, 31866; 1:1,000); β-actin (CST, 3700; 1:1,000) were diluted in TBS containing 0.05% Tween (TBST), 5% BSA and 0.02% NaN<sub>3</sub>. Membranes were incubated overnight with primary antibodies at 4 °C. For secondary antibody incubation, anti-rabbit HRP (Promega, W401B; 1:5,000) and anti-mouse HRP (Promega, W402B; 1:5,000) were diluted in TBST containing 1% milk. Results were visualized with enhanced chemiluminescence (ECL) western blotting substrates (Pierce, 32106).

#### Immunoprecipitation of SUMOylated protein for IP–MS

To detect SUMOylated proteins, samples were immunoprecipitated for 4 h at room temperature with anti-SUMO2/3 antibody (Abcam, ab81371; 2 µg of antibody per sample) that was coated on protein G magnetic beads (Invitrogen, 10007D). No antibody control samples were incubated with the protein G magnetic beads only. After incubation, the beads were washed 5 times with PBS and 2 times with water. Immunoprecipitated beads were resuspended with 200 mM EPPS and carried on-bead digest overnight at 37 °C by adding trypsin. Collected supernatants from each sample were transferred into a new tube. Samples were then labelled with 17-plex TMTpro reagents (Thermo) in 30% ACN/EPPS solution for an hour at room temperature. TMTpro-labelled peptides were mixed, then purified by C18 stage tip and analysed by LC–MS.

#### LC–MS analysis for SUMO IP–MS

An Orbitrap Eclipse Tribrid Mass Spectrometer (Thermo) coupled with an Easy-nLC1200 (Thermo) was used for proteomics analysis. A 120-min gradient consisting of 2%–35% ACN, 0.125% formic acid at 500 nL min<sup>-1</sup> flow rate was used to separate and analyse the peptides. Data-dependent acquisition was used mode using a mass range of *m/z* 400–1,600 using a 2 s cycle time method. Resolution for MS1 was set at 120,000. Singly-charged ions were not further sequenced, and multiply-charged ions were selected and subjected to fragmentation with standard automatic gain control and 35% NCE for MS2, with a dynamic exclusion window of 45 s. Quantification of TMTpro reporter ion were performed using the multinotch SPS-MS3 method<sup>53</sup> with 45% NCE for MS3.

#### Protein identification and data analysis for SUMO IP–MS

Raw files were processed using MaxQuant with an Andromeda search engine (ver. 2.1.2.0) against the human UniProt database (Swiss-Prot; retrieved 27 June 2022) as well as common contaminants. Peptides were searched using the following parameters: fully tryptic digestion up to three missed cleavages; variable modification: oxidation (+15.9949) of methionine and acetylation (+42.0106) on protein N-terminus, static modifications: TMTpro (+304.2071) on lysine and peptide N-terminus with a MS3 reporter ion type option setting. The FDR was set to <1% at protein level. Data analysis and visualization was done using InfernoRDN (v.1.1.7995) and Perseus (v.1.6.15.0). Data were first transformed to log<sub>2</sub> and central tendency adjustment normalization was carried out. Missing values were imputed by random numbers separately for

each column using a normal distribution with a down shifted value of 1.8 and width 0.3. Student t-test was carried for pairwise comparisons of variables.

#### Recombinant UBE2C generation

For UBE2C recombinant protein, pET-UbcH10-wt was a gift from J. Ruderman (Addgene, plasmid 8503)<sup>66</sup>. The 6×His-UBE2C plasmid was transformed into BL21 *Escherichia coli* (EMD Millipore). Three millilitres of overnight culture (50 mg ml<sup>-1</sup> kanamycin, TB broth) was used to inoculate 1 l of Overnight Express Instant TB Medium (Novagen) containing 50 mg ml<sup>-1</sup> kanamycin and grown for 24 h at 37 °C. Cells were then collected by centrifuging for 10 min at 6,000g, 4 °C and resuspended in 10 ml of 50 mM Tris, 500 mM NaCl, 1 mM TCEP, 10 mM imidazole, 1 tablet of cComplete, EDTA-free protease inhibitor cocktail, pH 8.0. Afterwards, the cells were lysed using tip sonication (30 s on, 30 s off, 6 cycles) and centrifuged for 30 min, at 25,000g, 4 °C. To the supernatant 2 ml of prewashed Ni-NTA Agarose beads (Qiagen) were added and rotated for 1 h at 4 °C. After draining the supernatant, the beads were then washed with 30 ml of 50 mM Tris, 500 mM NaCl, 1 mM TCEP, 10 mM imidazole, pH 8.0. Proteins were then eluted using 10 ml of 50 mM Tris, 500 mM NaCl, 1 mM TCEP, 200 mM imidazole, pH 8.0. The eluted proteins were then concentrated using a 3k-cut-off Amicon Ultra-15 Centrifugal Filter Units and after measuring the concentration using Pierce BCA protein assay kit, 6×His-UBE2C was then frozen at –80 °C.

#### Generation of recombinant SENP1, SENP3 and SENP5

pET28a-SENP1 (catalytic domain) was a gift from G. Salvesen, (Addgene, 16356)<sup>67</sup>. The N-terminal His tag construct of human SENP1 (residues 419–644) was overexpressed in *E. coli* BL21 (DE3) and purified using affinity chromatography and size-exclusion chromatography. In brief, cells were grown at 37 °C in TB medium in the presence of 50 µg ml<sup>-1</sup> of kanamycin to an *A*<sub>600</sub> of 0.8, cooled to 17 °C, induced with 500 µM isopropyl-1-thio-D-galactopyranoside (IPTG), incubated overnight at 17 °C, collected by centrifugation, and stored at –80 °C. Cell pellets were lysed in buffer A (25 mM HEPES, pH 7.5, 500 mM NaCl, 0.5 mM TCEP, and 20 mM Imidazole) using Microfluidizer (Microfluidics), and the resulting lysate was centrifuged at 30,000g for 40 min. Ni-NTA beads (Qiagen) were mixed with cleared lysate for 30 min and washed with buffer A. Beads were transferred to an FPLC-compatible column, and the bound protein was washed further with buffer A for 10 column volumes and eluted with buffer B (25 mM HEPES, pH 7.5, 500 mM NaCl, 0.5 mM TCEP, and 400 mM imidazole). N-terminal His was removed by incubating with thrombin overnight at 4 °C. The His tag cleaved sample was concentrated and purified further using a Superdex 200 16/600 column (Cytiva) in buffer C containing 20 mM HEPES, pH 7.5, 200 mM NaCl, and 0.5 mM TCEP. SENP1 containing fractions were concentrated to ~30 mg ml<sup>-1</sup> and stored in –80 °C. For SENP3 and SENP5 recombinant protein generation, pET28a-HsSENP3 (307–574, catalytic domain) (Addgene, 71481) and pET28a-SENP5 (catalytic domain) (Addgene, 16358) was overexpressed and purified as described above. For <sup>15</sup>N labelling, SENP1 was overexpressed in M9 medium supplemented with <sup>15</sup>N-NH<sub>4</sub>Cl (1 g l<sup>-1</sup>, Cambridge Isotope), induced with 500 µM IPTG for overnight at 17 °C, collected and stored at –80 °C. <sup>15</sup>N-labelled SENP1 was purified as described above. pET28a-HsSENP3 (307–574, catalytic domain) (Addgene, 71481) was a gift from J. E. Azevedo. pET28a-SENP5 (catalytic domain) (Addgene, 16358) was a gift from G. Salvesen. The N-terminal His tag constructs of human SENP3 and SENP5 were expressed and purified as described above for SENP1, except Tris (pH 8.0) buffers were used for Ni-affinity step in place of HEPES (pH 7.5) and thrombin cleavage step was omitted.

#### Generation of recombinant SENP2, SENP6 and SENP7

pET28a-SENP2/7 (catalytic domains) were gifts from G. Salvesen (Addgene, 16357 and 16360)<sup>67</sup>. The coding sequence for the SENP6 catalytic domain (Addgene, 16359) was cloned into an expression vector

# Article

with a TEV-cleavable N-terminal 6-His tag by ligation-independent cloning. For expression in *E. coli*, cells were grown to an  $A_{600}$  of ~0.5, and expression of N-terminally His<sub>6</sub>-tagged SENP2, SENP6 or SENP7 catalytic domain was induced by addition of IPTG (0.4 mM final concentration). Cultures were then incubated overnight at 18 °C before collecting by centrifugation and freezing at -80 °C in buffer D800 (20 mM HEPES, pH 7.5, 800 mM NaCl, 10 mM imidazole, 2 mM 2-mercaptoethanol, 10% glycerol by volume) (~6 ml per l of culture). Protease inhibitors aprotinin, leupeptin, pepstatin, benzamidine, and PMSF were added immediately before freezing. Cell pellets were thawed, treated with ~1 mg ml<sup>-1</sup> lysozyme (*E. coli* expression only), and sonicated for 2 min. After lysis, soluble material was recovered by centrifugation for 60 min at 12,000 rpm in a FA-45-6-30 rotor (Eppendorf). Proteins were purified from this extract by means of Co<sup>2+</sup> affinity chromatography. The Co<sup>2+</sup> resin eluate was applied to a 5 ml ion exchange column (GE HiTrap Q HP) equilibrated in buffer B50 and eluted by a five-column volume gradient into buffer D800. For SENP6 and SENP7, peak fractions were collected. SENP2 did not bind the ion exchange column, so the flow through was taken. Proteins were concentrated and further purified on a Superdex 200 column (10/300 GL, GE) equilibrated in gel filtration buffer (20 mM Tris-HCl, pH 8.5, 150 mM NaCl, 1 mM TCEP). Peak fractions were collected, concentrated by ultrafiltration, frozen in gel filtration buffer supplemented with 5% glycerol by volume, and stored at -80 °C until use.

## NMR studies on recombinant SENP1

All <sup>1</sup>H-<sup>15</sup>N-TROSY HSQC spectra were collected using ~100 μM wild-type SENP1 or SENP1(C535S) in buffer that contained 20 mM MES (2-(*N*-morpholino)ethanesulfonic acid), 50 mM NaCl, 1 mM TCEP at a pH of 6.5, supplemented with 10 % D<sub>2</sub>O for lock purposes. ZnSO<sub>4</sub> and sodium lactate were dissolved in the same buffer to generate stock solutions at a concentration of 60 mM and 500 mM, respectively. When required, appropriate amount of the stock solutions was added to the protein-containing samples to reach a final concentration of ZnSO<sub>4</sub> and Na-lactate as indicated. <sup>1</sup>H-<sup>15</sup>N-HSQC spectra were recorded on a Bruker Avance III 800 MHz spectrometer equipped with a TXO-style cryogenically cooled probe. Thirty-two scans and 128 complex points in the indirect <sup>15</sup>N dimension were collected at 298 K. The indirect dimension was sampled using an Echo-AntiEcho acquisition mode. NMR data was processed using nmrPipe<sup>68</sup> and analysed using the CCPNMR software (version 2.4.1)<sup>69</sup>.

## NMR assignment of SENP1<sub>419-644</sub>

To obtain backbone resonance assignment of SENP1 we performed a suite of triple resonance experiments on a perdeurated (<sup>2</sup>H-<sup>13</sup>C-<sup>15</sup>N-labelled) sample of SENP1<sub>419-644</sub>. The triple-labelled SENP1 was expressed in M9 minimal medium which was prepared as follows: 6 g Na<sub>2</sub>HPO<sub>4</sub>, 3 g KH<sub>2</sub>PO<sub>4</sub> and 0.5 g NaCl were dissolved in 1 l of <sup>2</sup>H<sub>2</sub>O in a dry-autoclaved glass beaker. Then, the appropriate antibiotic was added, as well as MgSO<sub>4</sub> anhydrous (final concentration = 2.5 mM), CaCl<sub>2</sub> anhydrous (final concentration = 0.1 mM), 2 g D-glucose-<sup>13</sup>C<sub>6</sub>-<sup>2</sup>H<sub>7</sub>, 1 g <sup>15</sup>NH<sub>4</sub>Cl and 100 μl of a 10,000× vitamin mix (5 g riboflavin, 5 g niacinamide, 5 g pyridoxine monohydrate and 5 g thiamine dissolved in 1 l ethanol). Twenty-five millilitres of LB medium was prepared in <sup>2</sup>H<sub>2</sub>O and sterile filtered after addition of the appropriate antibiotic. The medium was inoculated with ~10 colonies from freshly-transformed BI21-DE3 *E. coli*. This was incubated in a shaking incubator at 37 °C for ~8 h. In the evening, the culture was centrifuged at 3,000g for 10 min and resuspended in 50 ml of the modified M9 medium and grown at 37 °C overnight. The following morning, the modified M9 medium described above was inoculated with the overnight culture. The bacteria were grown in a shaking incubator at 37 °C to an  $A_{600}$  of ~0.4, after which the temperature was dropped to 20 °C. Protein expression was induced at an  $A_{600}$  of 0.7–0.9 with IPTG at a final concentration 0.5 mM and grown overnight (~12 h).

Triple resonance backbone experiments were recorded on a Bruker Avance III 800 MHz spectrometer with a TXO-style cryogenically cooled probe, operating at 800 MHz proton frequency at 298K. SENP1 was concentrated to a concentration of 1 mM in SENP1 NMR buffer (20 mM MES (2-(*N*-morpholino)ethanesulfonic acid), 50 mM NaCl, 1 mM TCEP at a pH of 6.5, supplemented with 10 % D<sub>2</sub>O). For backbone resonance assignment, a TROSY version of HNCA, HN(CO)CA, HNCACB, HNCO and HN(CA)CO experiments were recorded. In addition, we used a homonuclear decoupled version of the HNCA, where the Cα-Cβ coupling is selectively refocused. This results in amino-acid specific shapes in the Cα resonance which aids resonance assignment to mitigate spectral degeneracy<sup>70</sup>. All 3D spectra were acquired using non-uniform sampling with 10% sampling of the Nyquist grid using Poisson Gap Sampling<sup>71</sup>. The non-uniform sampling spectra were reconstructed and processed with hmsIS<sup>72</sup>. T2 relaxation experiments were recorded on a 100 μM <sup>15</sup>N-labelled SENP1 sample (with and without 100 μM ZnSO<sub>4</sub>) using a standard pulse sequence from the Bruker library with a transverse relaxation delay of 10 ms, 20 ms, 40 ms, 60 ms, 80 ms, 100 ms and 120 ms T2 relaxation delays in scrambled order. The relaxation delays were acquired in a scrambled fashion. NMR data was processed using nmrPipe<sup>68</sup> and analysed using CCPNMR software (version 2.4.1)<sup>69</sup>.

## Mapping zinc-coordinating cysteines on SENP1 by mass spectrometry

Quantification of zinc labelling by SENP1 cysteines was performed using an adapted mass spectrometry approach<sup>38</sup>. Recombinant SENP1 was diluted to 36.6 μM using 50 mM HEPES, pH 7, 150 mM NaCl, and 100 μM TCEP. ZnSO<sub>4</sub> was added at 5×. Afterwards, sodium lactate, D-lactate, or pyruvate (final concentration 1 mM), were added and incubated for 10 min. Then, 5 μl of 250 mM iodoacetamide (final concentration 25 mM), 0.5 μl of TCEP (final concentration 5 mM), 2.5 μl of 1 M HEPES pH 7 and 17 μl of water was added and incubated for 30 min in the dark. Afterwards, methanol chloroform precipitation was conducted and the resulting protein pellets were dissolved in 50 μl of 200 mM EPPS pH 8 containing 0.5 μg of trypsin and LysC for 18 h at 37 °C. TMTpro labelling was conducted by transferring 45 μl of the digested peptides into fresh tubes and then 16 μl of acetonitrile and 5 μl of TMTpro was added to each tube. After an hour-long incubation, 3 μl of 5% hydroxylamine was added and incubated for an additional 15 min. Then samples were then acidified with 20% formic acids, pooled, and diluted to 3 ml using 1% formic acid and desalting using a 50 mg C18 Sep-Pak. The eluted peptides were then concentrated using a speed vac and redissolved in 5% formic acid, 5% acetonitrile, 90% water and 2 μg was used for mass spectrometry analysis.

## Recombinant SENP activity

SENP1 activity was determined using assay buffer (150 mM NaCl, 50 mM HEPES pH 7.0), 60 nM SENP1 and 1.15 μM SUMO2-AMC (R&D, UL-758-050). To determine the effect of zinc or lactate on SENP1 activity, 60 nM of SENP1 protein was incubated with various concentrations of zinc sulfate or sodium lactate for 15 min prior to addition of AMC-labelled SUMO. To determine whether lactate changes the effect of zinc on SENP1 activity, 60 nM of SENP1 protein was first incubated with various concentrations of zinc sulfate for 10 min and then co-incubated with various concentrations of lactate for 5 min. The reaction was performed in black 96-well plates at 37 °C and released fluorescence was measured using a plate reader equipped for excitation wavelength of 380 nm and an emission wavelength of 460 nm. For SENP2, SENP3, SENP5, SENP6, and SENP7 activity determination, 150 nM, 800 nM, 1,200 nM, 50 nM, and 200 nM of protein, respectively, was incubated with zinc sulfate or/and sodium lactate. For experiments containing albumin, SENP1 protein was diluted with assay buffer containing albumin (final concentration of SENP1 protein and albumin is 60 nM and 20 mg ml<sup>-1</sup>, respectively). After incubation with 120 nM zinc sulfate for 10 min, SENP1 protein was

co-incubated with various concentrations of sodium lactate for 5 min, followed by measuring released fluorescence.

### Molecular modelling of SENP1

The crystal structure of SENP1 (PDB: 2IYD) was used for building the models for Zn<sup>2+</sup> binding and Zn<sup>2+</sup>-lactate complex. The SUMO2 chain that was covalently linked to SENP1 was removed prior to model the structure complexes. After surveying multiple structures of SENP1 in the PDB database, the structures of SENP1 were very conserved in terms of conformation. The protein structure was prepared using Schrodinger suite (release 2021-2) with default parameters. Zn<sup>2+</sup> was initially placed at the centre of Cys535, His533, and Cys603, with both cysteines deprotonated. The initial configuration was then optimized using QM/MM method QSite from Schrodinger suite. The quantum region included Zn<sup>2+</sup>, side chains of His533, Asp550, Cys603 and the entire Cys535. The LACVP\* basis set and B3LYP exchange-correlation functional were chosen for DFT quantum calculations, and classical region was modelled by OPLS\_2005 forcefield. Initial optimization resulted in Cys603 being ejected from Zn<sup>2+</sup> coordination. The subsequent optimization was continued from neutralized Cys603 till convergency. The same calculation was performed for deprotonated Cys603 calculation but convergency was not obtained. To model lactate-bound complex, induced-fit docking was initially employed on the optimized Zn<sup>2+</sup> complex obtained from the previous step. The dominant binding mode was then further optimized by QM/MM method where lactate was included in the quantum region in addition to Zn<sup>2+</sup>, residue Cys535 and side chain of Asp550. His533 was excluded from quantum region in the optimization as it was no longer coordinating with Zn<sup>2+</sup> ion. Same basis set and exchange-correlation functional were used in the quantum optimization calculations.

### Generation of SENP1 mutant cell line

To generate the endogenous SENP1 N556A mutant cell line, we designed gBlock gene fragments containing sgRNA sequences as follows: CCTA TTACGACTCCATGGGT. And we designed SSODN sequences as HDR template as follows: TTTAGAAAGAAGAATATTACCTATTACGACAGC ATGGGTGGAATAGCCAATGAAGCCTGCAGAATACTCTTGTAACTAGGG AGTTGAGGACA. Then, PX458 vector, gBlock gene fragments, SSODN and HDR Enhancer v2 (from IDT) were nucleofected into HCT116 with Amaxa Cell Line Nucleofector Kit V (Lonza, VCA-1003) and Amaxa Nucleofector 2b machine. Using green fluorescent protein (GFP) as fluorochrome selection tag, cells were sorted by flow cytometry 48 h post-transfection. After 3 weeks, the isolated cell colony was validated for sequencing and SENP1 expression by immunoblot analysis.

### Analysis of lactate abundance in Cancer Cell Line Encyclopedia

Correlation between intracellular lactate abundance and doubling time in human proliferative cancers was analysed by using data from 707 human cancer cell lines<sup>46</sup>. Pearson's R value and P value were calculated based on the significance test of Pearson correlations (two-sided).

### Treatment of cells with oligomycin A, DCA, $\alpha$ -CHCA and GSK2837808A

HCT116 and HeLa S3 cells were seeded at a density of 400,000 cells per well in 6-well plates (for western blotting) or 200,000 cells per well in 12 well plate (for metabolomics), 24 h prior to use. Cells were collected after incubation with oligomycin A (Selleck, S1478) 1  $\mu$ M or  $\alpha$ -CHCA (Selleck, S8612) 5 mM for 24 h, followed by downstream experiments. For LDH inhibitor treatment, cells were collected after incubation with 10  $\mu$ M GSK2837808A (Thermo Fisher Scientific, 518910) and 15 mM sodium lactate for 4h, followed by western blotting. For DCA treatment, cells were synchronized with thymidine for twice as described above, then collected after being released into normal medium for 0, 2, 4, 6,

8, 10, 12, 14 or 16 h in the presence or absence of 25 mM DCA (Sigma Aldrich, 347795), followed by western blotting.

### Metabolite analyses by mass spectrometry

Metabolites were profiled using an LC-MS system comprised of a Nexera X2 U-HPLC (Shimadzu Scientific Instruments) coupled to a Q Exactive-HF-X orbitrap mass spectrometers (Thermo Fisher Scientific). Cells were rapidly isolated and homogenized in extraction solution of 80% methanol containing inosine-<sup>15</sup>N<sub>4</sub>, thymine-d<sub>4</sub> and glycocholate-d<sub>4</sub> internal standards (Cambridge Isotope Laboratories). 30  $\mu$ l of each homogenate was diluted in a further 120  $\mu$ l extraction solution. The samples were centrifuged (10 min, 9,000g, 4 °C) and the supernatants were injected directly onto a 150 × 2.0 mm Luna NH<sub>2</sub> column (Phenomenex). The column was eluted at a flow rate of 400  $\mu$ l min<sup>-1</sup> with initial conditions of 10% mobile phase A (20 mM ammonium acetate and 20 mM ammonium hydroxide in water) and 90% mobile phase B (10 mM ammonium hydroxide in 75:25 v/v acetonitrile/methanol) followed by a 10 min linear gradient to 100% mobile phase A. Mass spectrometry analyses were carried out using electrospray ionization in the negative ion mode using full scan analysis over m/z 60–750 at 70,000 resolution and 3 Hz data acquisition rate. Additional mass spectrometry settings were: ion spray voltage, -3.0 kV; capillary temperature, 350 °C; probe heater temperature, 325 °C; sheath gas, 55; auxiliary gas, 10; and S-lens RF level 40. Raw data were processed using Progenesis QI software (NonLinear Dynamics) for feature alignment, nontargeted signal detection, and signal integration. Targeted processing of a subset of known metabolites and isotopologues was conducted using TraceFinder software (Thermo Fisher Scientific). Compound identities were confirmed using reference standards.

### Cell cycle monitoring experiments

For double thymidine block, cells were synchronized with thymidine for twice as described above, then collected after being released into normal medium for 0, 2, 4, 6, 8, 10 or 12 h. For T cells experiments, CD8<sup>+</sup> T cells were collected at 2, 16 and 24 h following stimulation with proliferative cytokines as described above. At different time points, cells were collected and fixed overnight in cold 70% ethanol. Cells were then treated with 0.2 mg ml<sup>-1</sup> RNase A (Invitrogen, 12091021) at 37 °C for 1 h, followed by incubation with 2  $\mu$ g ml<sup>-1</sup> propidium iodide (Invitrogen, P3566) and analysis with FACS.

### Cellular proliferation assay

HeLa S3 and HCT116 wild-type and APC4(K772/798R) cells were seeded at a density of 300,000 and 200,000 cells per well in a 6-well plate, respectively one day prior to use. Cells were detached using trypsin and then were resuspended with fresh complete medium. Number of cells was counted at 1, 2, 3, 4 and 5 days after the beginning of the experiment with countess 3 cell counters (Invitrogen).

### Assessing gene expression by qPCR

HCT116 and HeLa S3 cells were scraped into TRIzol reagent (Thermo Fisher Scientific, 15596018) and RNA was extracted into chloroform followed by addition of 70% ethanol. RNA was purified using the PureLink RNA Mini Kit (Invitrogen, 12183018A). RNA was quantified using a NanoDrop One UV-vis spectrophotometer (Thermo Fisher Scientific). 1000 ng of RNA was used to synthesize cDNA by PCR with reverse transcription using the high-capacity cDNA Reverse Transcription Kit (Thermo Fisher Scientific, 4368814). cDNA was then diluted in a 1:10 ratio cDNA to nuclease-free water and used for qPCR analysis. The qPCR reaction was performed in 384 well plates using the GoTaq qPCR Master Mix (Promega, A6001). Samples were amplified on a Quant Studio 6 Flex Real-Time PCR machine (Applied Biosystems). Relative abundance of gene was calculated by the  $\Delta Ct$  or  $2^{-\Delta\Delta Ct}$  method using ACTB as an endogenous reference.

## Primers for qPCR analysis

*LMO* forward, AGCACACAGAGGGCTAAC, reverse, CCGATGGGA GCGAAGAACAT; *Foxk1* forward, CAGTACCGCTTGTCAGAA, reverse, CGGCTTGACTCATCCTTGG; *Foxk2* forward, AAGAACGGGGT ATTCTGTGGAC, reverse, CTCGGAACCTGAATGTGC.

## Statistical analyses

Data were expressed as mean  $\pm$  s.e.m. and *P* values were calculated using two-tailed Student's *t*-test for pairwise comparison of variables, one-way ANOVA for multiple comparison of variables, and two-way ANOVA for multiple comparisons involving two independent variables. ANOVA analyses were subjected to Bonferroni's post hoc test. Sample sizes were determined on the basis of previous experiments using similar methodologies. For all experiments, unless otherwise stated, all stated replicates are biological replicates. For cell and cell lysate experiments, each biological replicate originated from a shared genetically validated stock, was independently plated, cultured for at least 48 h, and independently replated prior to the experiment. For mass spectrometry analyses, samples were processed in random order and experimenters were blinded to experimental conditions.

## Reporting summary

Further information on research design is available in the Nature Portfolio Reporting Summary linked to this article.

## Data availability

Mass spectrometry proteomics data have been deposited to the ProteomeXchange Consortium via the PRIDE partner repository with the dataset identifier PXD036641. NMR backbone resonance assignments of SENP1 have been deposited to the Biological Magnetic Resonance Bank and can be accessed with the accession code 51766. All data associated with this work are otherwise provided in the manuscript, and will be provided upon request to the corresponding author. Source data are provided with this paper.

52. Schweppke, D. K. et al. Characterization and optimization of multiplexed quantitative analyses using high-field asymmetric-waveform ion mobility mass spectrometry. *Anal. Chem.* **91**, 4010–4016 (2019).
53. McAlister, G. C. et al. MultiNotch MS3 enables accurate, sensitive, and multiplexed detection of differential expression across cancer cell line proteomes. *Anal. Chem.* **86**, 7150–7158 (2014).
54. Eng, J. K., Jahan, T. A. & Hoopmann, M. R. Comet: an open-source MS/MS sequence database search tool. *Proteomics* **13**, 22–24 (2013).
55. Huttlin, E. L. et al. A tissue-specific atlas of mouse protein phosphorylation and expression. *Cell* **143**, 1174–1189 (2010).
56. Elias, J. E. & Gygi, S. P. Target-decoy search strategy for increased confidence in large-scale protein identifications by mass spectrometry. *Nat. Methods* **4**, 207–214 (2007).
57. Peng, J., Elias, J. E., Thoreen, C. C., Licklider, L. J. & Gygi, S. P. Evaluation of multidimensional chromatography coupled with tandem mass spectrometry (LC/LC-MS/MS) for large-scale protein analysis: the yeast proteome. *J. Proteome Res.* **2**, 43–50 (2003).
58. Beausoleil, S. A., Villen, J., Gerber, S. A., Rush, J. & Gygi, S. P. A probability-based approach for high-throughput protein phosphorylation analysis and site localization. *Nat. Biotechnol.* **24**, 1285–1292 (2006).
59. Franken, H. et al. Thermal proteome profiling for unbiased identification of direct and indirect drug targets using multiplexed quantitative mass spectrometry. *Nat. Protoc.* **10**, 1567–1593 (2015).
60. Mateus, A., Maatta, T. A. & Savitski, M. M. Thermal proteome profiling: unbiased assessment of protein state through heat-induced stability changes. *Proteome Sci.* **15**, 13 (2016).

61. Whitfield, M. L. et al. Stem-loop binding protein, the protein that binds the 3' end of histone mRNA, is cell cycle regulated by both translational and posttranslational mechanisms. *Mol. Cell. Biol.* **20**, 4188–4198 (2000).
62. Chen, G. & Deng, X. Cell synchronization by double thymidine block. *Bio Protoc.* **8**, e2994 (2018).
63. Wang, T. et al. Succinate induces skeletal muscle fiber remodeling via SUNC1 signaling. *EMBO Rep.* **20**, e47892 (2019).
64. Chen, W. W., Freinkman, E., Wang, T., Birsoy, K. & Sabatini, D. M. Absolute quantification of matrix metabolites reveals the dynamics of mitochondrial metabolism. *Cell* **166**, 1324–1337.e1311 (2016).
65. Cantor, J. R. et al. Physiologic medium rewires cellular metabolism and reveals uric acid as an endogenous inhibitor of UMP synthase. *Cell* **169**, 258–272.e217 (2017).
66. Bastians, H., Topper, L. M., Gorbsky, G. L. & Ruderman, J. V. Cell cycle-regulated proteolysis of mitotic target proteins. *Mol. Biol. Cell* **10**, 3927–3941 (1999).
67. Mikolajczyk, J. et al. Small ubiquitin-related modifier (SUMO)-specific proteases: profiling the specificities and activities of human SENPs. *J. Biol. Chem.* **282**, 26217–26224 (2007).
68. Delaglio, F. et al. NMRPipe: A multidimensional spectral processing system based on UNIX pipes. *J. Biomol. NMR* **6**, 277–293 (1995).
69. Vranken, W. F. et al. The CCPN data model for NMR spectroscopy: development of a software pipeline. *Proteins* **59**, 687–696 (2005).
70. Coote, P. W. et al. Optimal control theory enables homonuclear decoupling without Bloch-Siegert shifts in NMR spectroscopy. *Nat. Commun.* **9**, 3014 (2018).
71. Hyberts, S. G., Takeuchi, K. & Wagner, G. Poisson-gap sampling and forward maximum entropy reconstruction for enhancing the resolution and sensitivity of protein NMR data. *J. Am. Chem. Soc.* **132**, 2145–2147 (2010).
72. Hyberts, S. G., Milbradt, A. G., Wagner, A. B., Arthanari, H. & Wagner, G. Application of iterative soft thresholding for fast reconstruction of NMR data non-uniformly sampled with multidimensional Poisson gap scheduling. *J. Biomol. NMR* **52**, 315–327 (2012).

**Acknowledgements** This work was supported by the Claudia Adams Barr Program (E.T.C.), the Lavine Family Fund (E.T.C.), the Pew Charitable Trust (E.T.C.), NIH DK123095 (E.T.C.), NIH AG071966 (E.T.C.), The Smith Family Foundation (E.T.C.), the American Federation for Aging Research (E.T.C.), the American Heart Association (L.H.M.B.), NIH DK123321 (E.L.M.), the National Cancer Center (H.X.), NIH K99AG073461 (H.X.), the Deutsche Forschungsgemeinschaft (DFG, German research foundation) Projektnummer 501493132 (N.B.), the Linde Family Foundation (S.D.-P.), the Doris Duke Charitable Foundation (S.D.-P.), Deerfield 3DC (S.D.-P.), Taiho Pharmaceuticals (S.D.-P.), the Hope Funds for Cancer Research HFCR-20-03-01-02 (H.-G.S.), NIH GM136859 (H.A.), and The Smith Family Foundation (H.A.). The authors thank M. Kirschner, R. King, B. Spiegelman, M. Murphy and W. Harper for helpful discussion; N. Brown for providing structural models of APC/C; and B. V. Carolos for providing the LMO construct. Cartoon illustrations in Fig. 4h and Extended Data Figs. 1b,c,e, 5a,b,h and 6a were created with BioRender.com.

**Author contributions** W.L. and E.T.C. conceived of and designed the study. W.L., Y.W. and L.H.M.B. performed cellular experiments and analysed data. M.P.J., H.X. and N.D. carried out and analysed data from mass spectrometry experiments. P.F. performed and analysed data from NMR experiments. S.W. and E.L.M. carried out thermal proteome profiling experiments. T.W. assisted with design of APC/C experiments. N.D. assisted with protein expression and purification. X.H. assisted with time-lapse microscopy. E.L.M. performed T cells experiments and metabolomics experiments. N.B. assisted with LMO overexpression and metabolomics experiments. S.S. performed SUMO proteomics experiments. A.R. carried out and analysed data from metabolomics experiments and assisted with experiments under hypoxia. H.-G.S. performed cellular volume experiments. S.M.H. assisted with the expression and purification of SENP proteins. N.T. assisted with the construction of plasmids. J.S. assisted with design of mitosis and proliferation experiments. H.-S.S. carried out SENP1 expression and purification. K.S., A.Z.X. and L.S. assisted with SENP1 expression and purification. J.J.Z. oversaw time-lapse microscopy. S.D.-P. oversaw SENP1 expression and purification. J.C. performed molecular modelling. H.A. oversaw NMR experiments. S.P.G. oversaw mass spectrometry experiments. E.T.C. directed the research, oversaw the experiments, and wrote the manuscript with assistance from the other authors.

**Competing interests** J.Z. is co-founder and board director of Crimson Biopharm Inc. and Geode Therapeutics Inc. E.T.C. is co-founder of Matchpoint Therapeutics and Aevum Therapeutics. J.C. is a co-founder for Matchpoint Therapeutics. J.C. is a scientific co-founder M3 Bioinformatics & Technology Inc., and consultant and equity holder for Soltego and Alliorion. All other authors declare no competing interests.

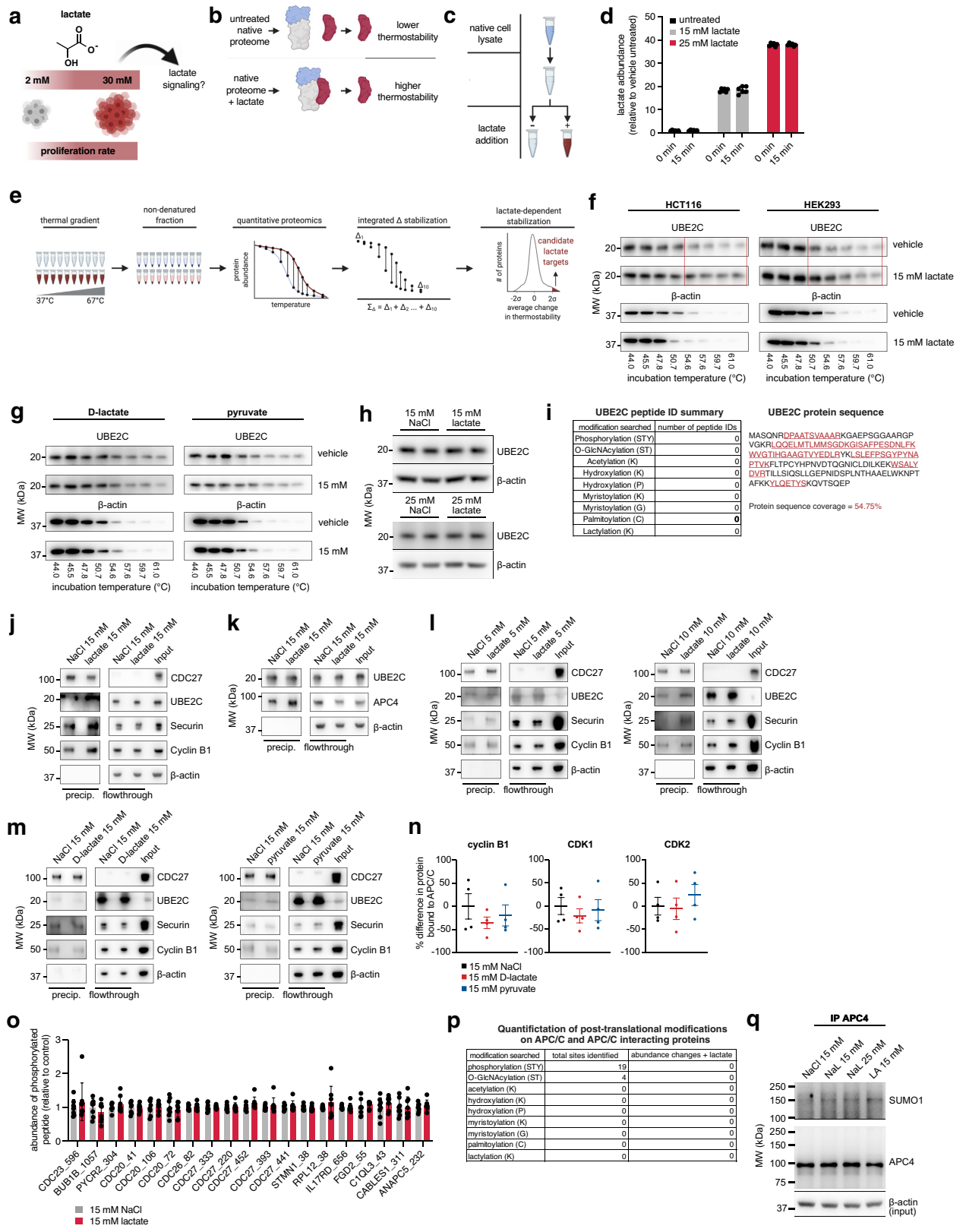
## Additional information

**Supplementary information** The online version contains supplementary material available at <https://doi.org/10.1038/s41586-023-05939-3>.

**Correspondence and requests for materials** should be addressed to Edward T. Chouchani.

**Peer review information** *Nature* thanks Jordan Meier and the other, anonymous, reviewer(s) for their contribution to the peer review of this work.

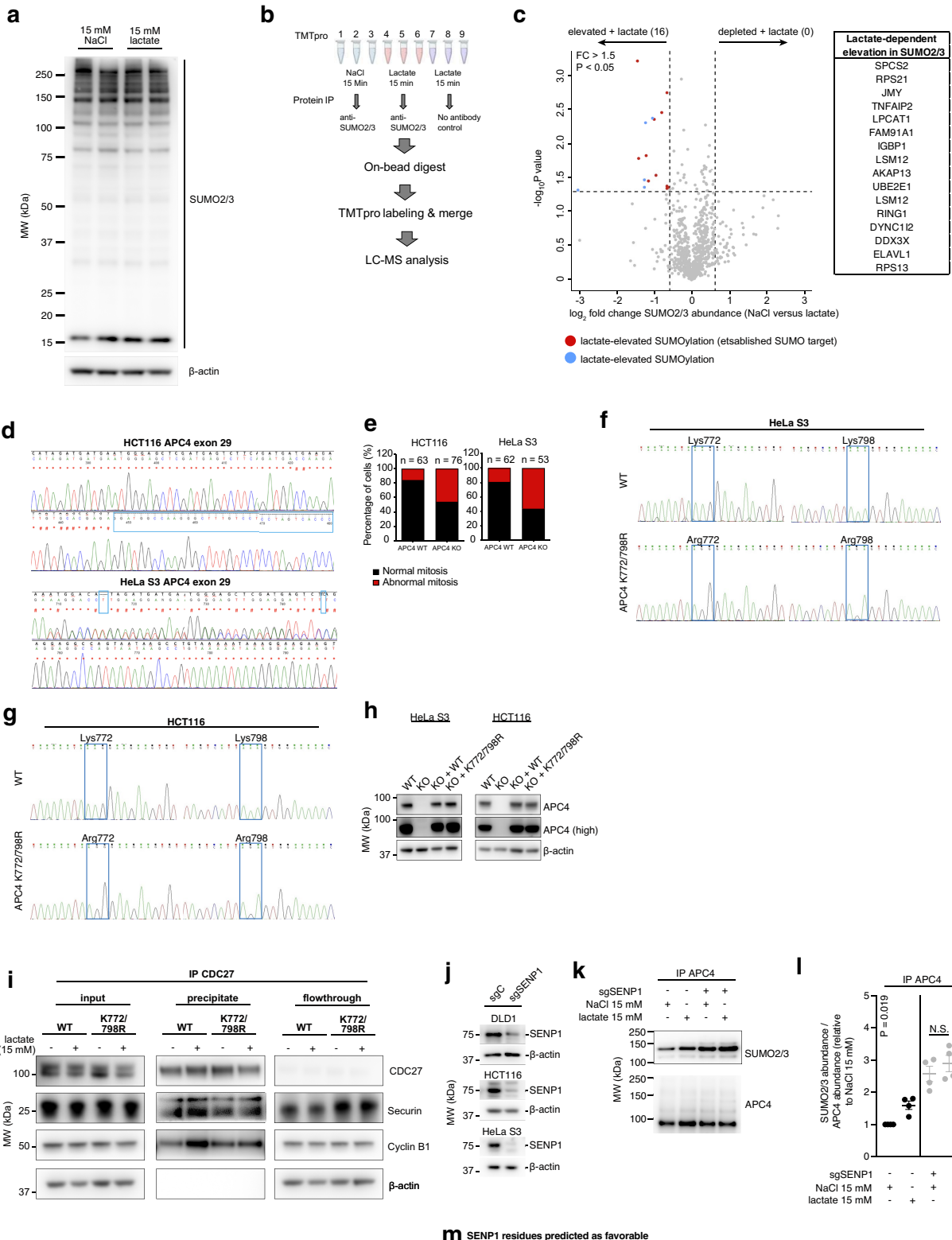
**Reprints and permissions information** is available at <http://www.nature.com/reprints>.



**Extended Data Fig. 1** | See next page for caption.

# Article

**Extended Data Fig. 1 | Molecular consequences of elevated lactate on UBE2C and APC/C.** (a) Hypothesis that high lactate concentration can directly regulate cellular processes. (b) Outline of the principle that TPP can reveal lactate mediated changes in protein thermostability through acquired protein-protein interactions. (c) Acute treatment of native HEK proteomes with lactate following cell lysis and dilution. (d) Stable abundance of lactate in HEK293 cellular lysates over 15 min incubation period used for TPP experiment. n = 6 cell replicates. (e) TPP workflow to assess proteome-wide changes in protein thermostability following lactate treatment. (f) Thermostability changes to UBE2C in HEK293 and HCT116 cell lysates following treatment with lactate, as determined by western blotting. Representative blot from three experiments shown. (g) Lack of observable thermostability changes to UBE2C in HCT116 cell lysates following treatment with D-lactate or pyruvate. Representative blot from three experiments shown. (h) Effect of acute (15 min) elevation of lactate on UBE2C protein abundance in cellular lysates. Representative blot from two experiments shown. (i) Effect of acute (15 min) elevation of lactate on post-translational modifications of UBE2C. (j) IP of pro-metaphase APC(CDC27) following lactate treatment without addition of exogenous UBE2C demonstrates lactate-mediated binding of UBE2C, cyclin B1, and securin to pro-metaphase APC/C. Representative blot from two experiments shown. (k) IP of UBE2C following lactate treatment demonstrates lactate-mediated binding of UBE2C to APC/C as determined by blotting for APC4. Representative blot from two experiments shown. (l) IP of pro-metaphase APC(CDC27) following 5 mM and 10 mM lactate treatment to determine effect on binding of UBE2C, cyclin B1, and securin to pro-metaphase APC/C. (m) IP of pro-metaphase APC(CDC27) following D-lactate (left) or pyruvate (right) treatment demonstrates no effect on binding of UBE2C, cyclin B1, and securin to pro-metaphase APC/C. (n) IP-MS of APC(CDC27) following D-lactate or pyruvate treatment demonstrates lack of effect on binding of Cyclin B1, CDK1, and CDK2. n = 4 cell replicates. (o) Quantification of phosphorylation on APC/C, and APC/C interacting proteins, following cell lysate incubation with 15 mM lactate. n = 8 cell replicates. (p) Effect of acute (15 min) elevation of lactate on post-translational modifications of APC/C, and APC/C interacting proteins. n = 8 cell replicates. (q) SUMO1 (top) and APC4 (bottom) immunoblot of immunopurified APC4 following lactate treatment in intact cells for 4 h. Representative blot from two experiments shown. Data are mean ± s.e.m.



**m** SENP1 residues predicted as favorable for zinc binding

Asp468 His491 Asp517 His529  
His533 Cys535 Cys603

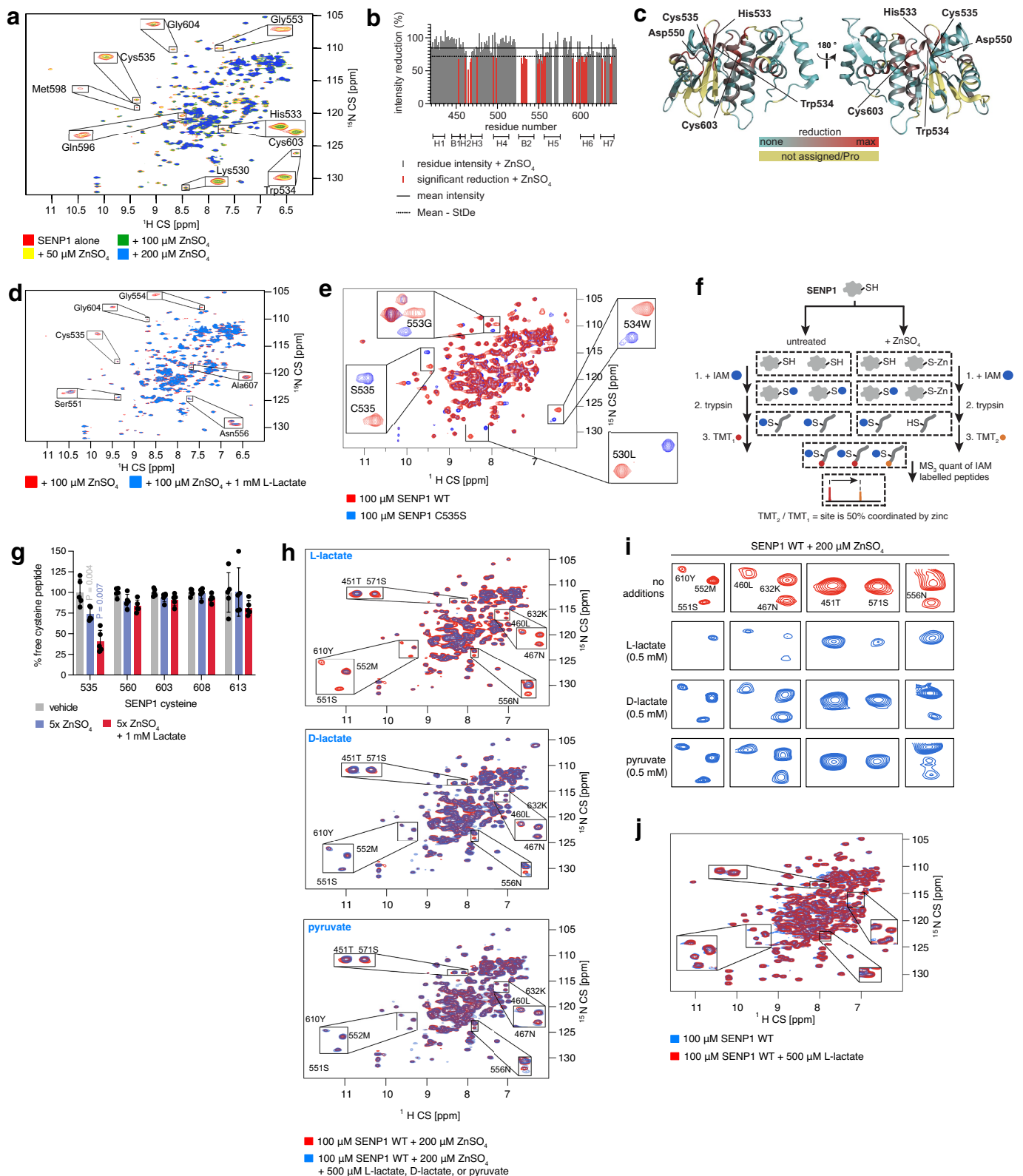
Extended Data Fig. 2 | See next page for caption.

# Article

## Extended Data Fig. 2 | Characterization of lactate-dependent APC4 SUMOylation.

**(a)** Effect of 15 min lactate treatment on total SUMO2/3 content in cellular lysates. Representative blot from two experiments shown. **(b)** Experimental design for identification of protein SUMOylation that is elevated in response to lactate. See Methods for details. **(c)** Quantification of differential SUMOylation of 860 proteins following treatment of HCT116 cell lysates with 15 mM lactate for 15 min. 16 proteins exhibiting significant lactate-dependent elevation in SUMOylation are highlighted. n = 3 cell replicates. **(d)** Sequencing of APC4 gene locus in APC4 KO HeLa S3 and HCT116 cells. In both cases, the relevant region of exon 29 is shown highlighting nucleotide differences (#) to WT sequence (black) and frameshift mutations that elicited KO (blue squares). In HeLa S3 cells the highlighted region indicates two distinct frame shift mutations. **(e)** APC4 KO cells exhibit abnormal mitosis. Method for defining abnormal mitosis described in the Methods section. **(f)** Sequencing of APC4 in HeLa S3 expressing lentiviral WT and mutant constructs containing WT sequence APC4 K772 & K798, and mutant R772 & R798. **(g)** Sequencing of APC4 in HCT116 expressing lentiviral WT and mutant constructs containing WT sequence APC4 K772 & K798, and mutant R772 & R798. **(h)** APC4 immunoblot

of HeLa S3 and HCT116 WT, APC4 KO, and APC4 KO cells re-expressing WT APC4 or APC4 K772/798R. Representative blot from three experiments shown. **(i)** IP of APC(CDC27) following lactate treatment in cell lysates demonstrates lactate-mediated binding of cyclin B1 and securin to pro-metaphase APC/C requires APC4 SUMO2/3 targets K772 and K798. Representative blot from three experiments shown. **(j)** CRISPR depletion of SENP1 in three proliferative human cell lines. sgC: guide control. Representative blot from two experiments shown. **(k)** SUMO2/3 (top) and APC4 (bottom) immunoblot of immunopurified APC4 following lactate treatment in cells for 4 h in WT and SENP1KO cells indicates lack of additive effect, suggesting the modalities operate in series. Representative blot from four experiments shown. **(l)** Densitometry quantification immunoblot replicates from panel k immunopurified APC4 following lactate treatment in WT and SENP1KO cells indicates lack of additive effect, suggesting the modalities operate in series. n = 4 cell replicates. **(m)** SENP1 residues predicted as favorable for zinc binding according to ZincBind algorithm using SENP1 structure PDB 2XPH. (two-tailed Student's t-test for pairwise comparisons in l). ANOVA analyses were subjected to Bonferroni's post hoc test. Data are mean ± s.e.m.



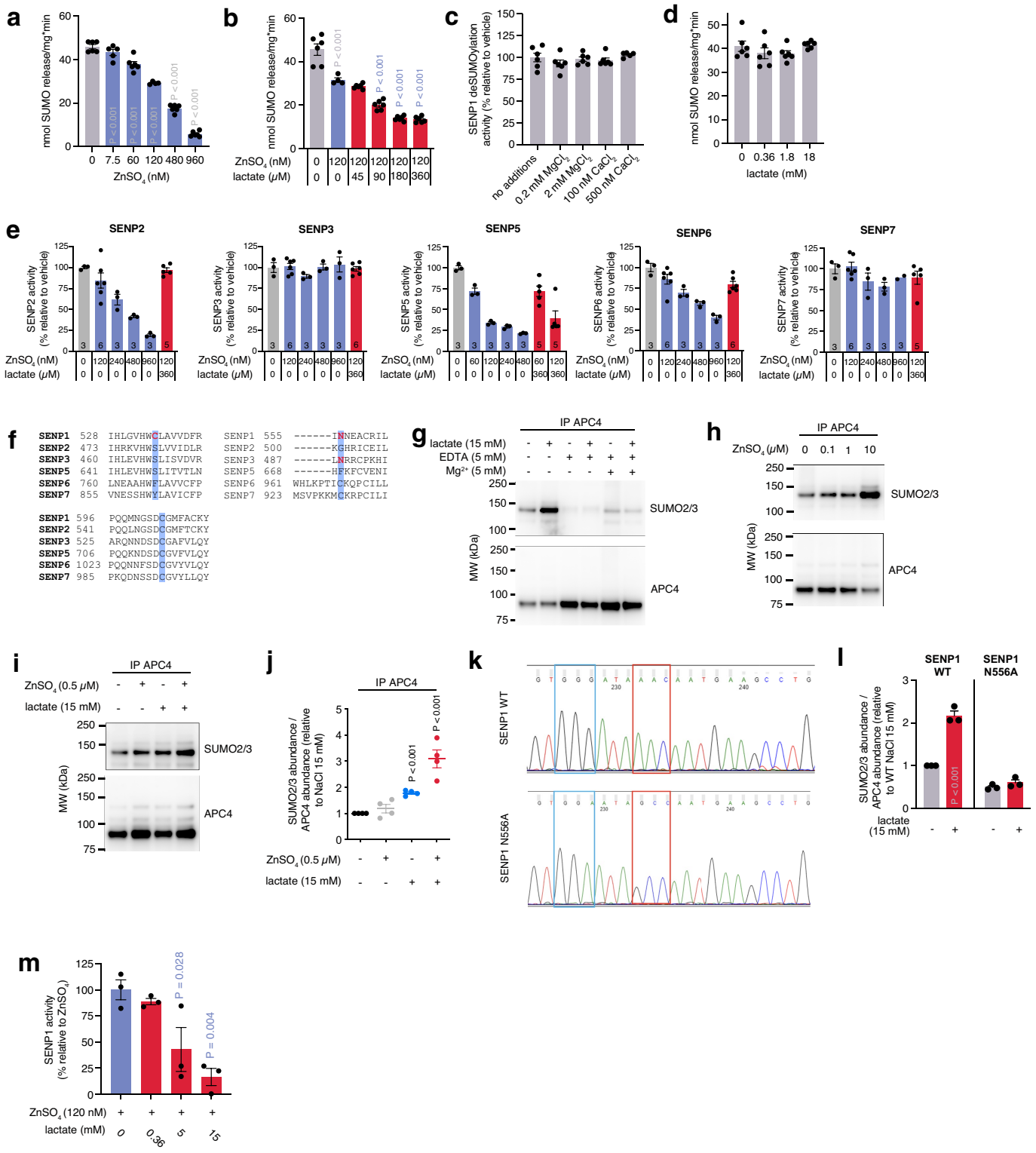
**Extended Data Fig. 3** | See next page for caption.

# Article

## Extended Data Fig. 3 | Characterization of lactate and zinc binding to SENP1.

(a)  $^1\text{H}$ - $^{15}\text{N}$  TROSY HSQC spectrum of SENP1<sub>419-644</sub> +/- zinc binding, highlighting all active site regions. (b) Intensity reduction in SENP1 resonances as a function of residue number after addition of 100  $\mu\text{M}$  zinc to SENP1. (c) Structure of SENP1 (PDB ID 2IYC) color-coded as a heatmap according to peak intensity reduction caused by the addition of 100  $\mu\text{M}$  zinc (cyan = no intensity reduction, red = maximum intensity reduction). (d)  $^1\text{H}$ - $^{15}\text{N}$  TROSY HSQC spectra of SENP1<sub>419-644</sub> + 100  $\mu\text{M}$  zinc and +/- 1 mM L-lactate, highlighting active site residues. (e)  $^1\text{H}$ - $^{15}\text{N}$  HSQC spectrum of human SENP1 catalytic domain comparing WT protein to C535S mutant. Spectral shifts differentiating WT and C535S SENP1 that match assignment to C535 in annotated spectra are highlighted. (f) MS determination and quantification of SENP1 cysteines that coordinate zinc. Method reports on stoichiometry of zinc binding with individual cysteines based on differential

labelling with iodoacetamide (IAM)<sup>38</sup>. See Methods for details. (g) Quantification of zinc binding to human SENP1 cysteines by MS  $\pm$  1 mM lactate. Stoichiometry of zinc labelling of cysteines determined as described in Extended Data Fig. 3f, n = 5 independent samples. (h)  $^1\text{H}$ - $^{15}\text{N}$  HSQC spectrum of human WT SENP1  $\pm$  ZnSO<sub>4</sub> in the presence or absence of 0.5 mM L-lactate, D-lactate, or pyruvate. Active site residues where L-lactate+zinc induced CSPs are observed are highlighted. (i)  $^1\text{H}$ - $^{15}\text{N}$  NMR spectra regions of WT SENP1 comparing L-lactate+zinc induced active site CSPs to D-lactate and pyruvate. (j)  $^1\text{H}$ - $^{15}\text{N}$  HSQC spectrum of human WT SENP1  $\pm$  0.5 mM lactate. Regions of the spectrum where L-lactate+zinc induced CSPs in the active site are highlighted showing none of these CSPs occur in the absence of zinc. (one-way ANOVA for multiple comparisons in g. ANOVA analyses were subjected to Bonferroni's post hoc test). Data are mean  $\pm$  s.e.m.

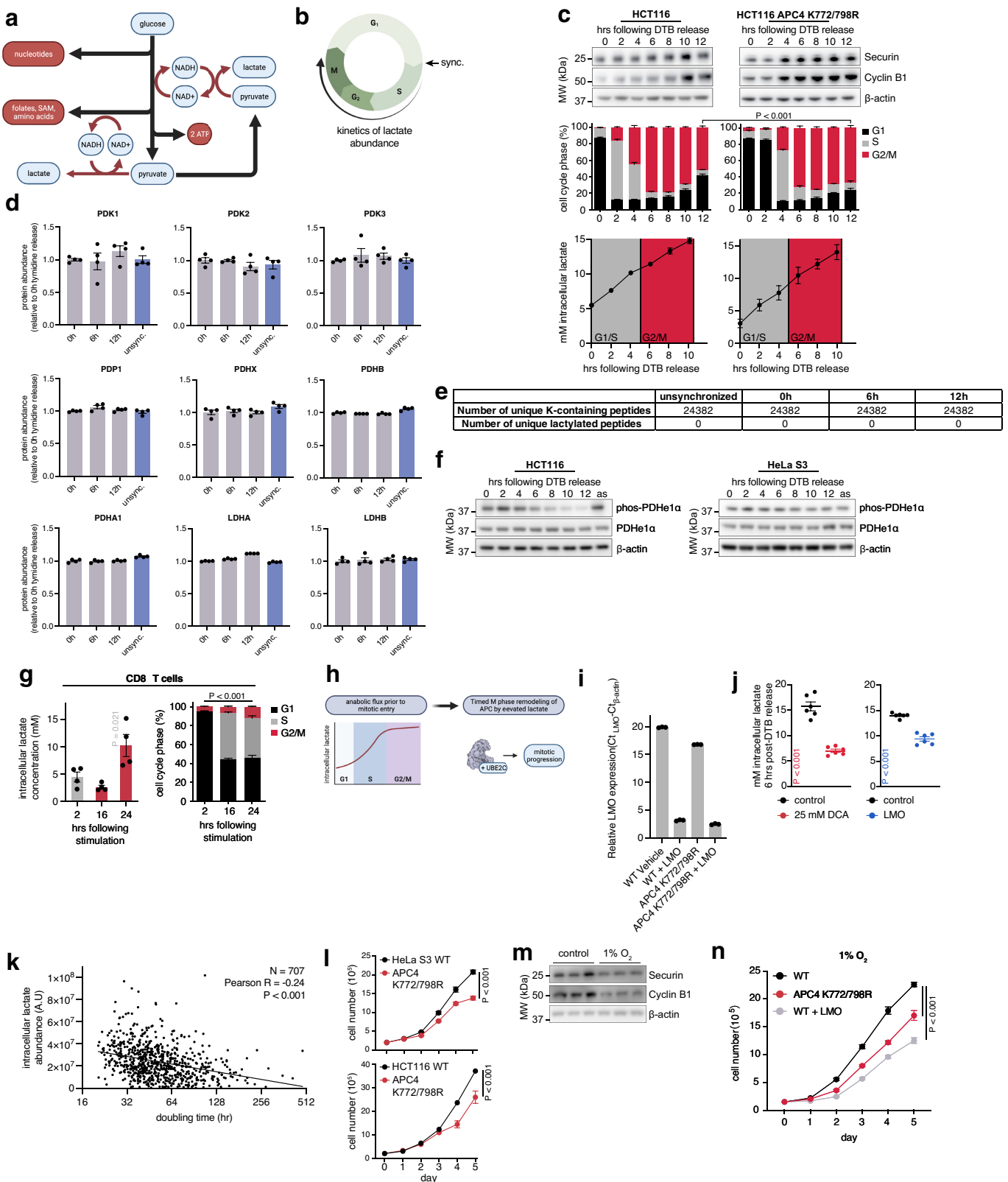


**Extended Data Fig. 4** | See next page for caption.

# Article

**Extended Data Fig. 4 | Characterization of functional effects of lactate and zinc on SENP family.** (a) Effect of ZnSO<sub>4</sub> on recombinant human SENP1 deSUMOylation activity. n = 6; 7.5 nM n = 5 independent samples. (b) Effect of lactate on zinc-mediated inhibition of recombinant SENP1 deSUMOylation activity. n = 6; 120 nM zinc n = 4 independent samples. (c) Effect of MgCl<sub>2</sub> and CaCl<sub>2</sub> on recombinant human SENP1 deSUMOylation activity. n = 6; 500 nM CaCl<sub>2</sub> n = 5 independent samples. (d) Effect of lactate on recombinant human SENP1 deSUMOylation activity. n = 6 independent samples. (e) Effect of ZnSO<sub>4</sub> and lactate on recombinant human SENP2, SENP3, SENP5, SENP6, and SENP7 deSUMOylation activity. n shown in panel and indicate independent samples. (f) Sequence alignment of human SENP family active site regions highlighting residues involved in SENP1 co-ordination of lactate-zinc complex (C535 and N556). (g) SUMO2/3 (top) and APC4 (bottom) immunoblot of immunopurified APC4 following lactate treatment in cellular lysates in the presence of EDTA to chelate zinc, including supplementation with Mg<sup>2+</sup> to control for effects of EDTA on Mg<sup>2+</sup> chelation. Representative blot from three experiments shown. (h) SUMO2/3 (top) and APC4 (bottom) immunoblot of immunopurified APC4

following ZnSO<sub>4</sub> treatment in cellular lysates demonstrate that elevation of zinc stabilizes APC4 SUMOylation. Representative blot from three experiments shown. (i) SUMO2/3 (top) and APC4 (bottom) immunoblot of immunopurified APC4 following treatment with sub-optimal zinc and lactate in cellular lysates. Representative blot from four experiments shown. (j) Densitometry quantification immunoblot replicates from panel i of immunopurified APC4 following suboptimal zinc treatment in the presence or absence of lactate. n = 4 cell replicates. (k) Sequencing of SENP1 in HCT116 expressing lentiviral WT and mutant constructs containing WT sequence N556, and mutant A556. Blue region highlights silent PAM mutation, red region highlights N556A mutation. (l) Densitometry of immunopurified APC4 following lactate treatment in cellular lysates from SENP1 WT and N556A HCT116 cells, related to Fig. 3k. (m) Effect of lactate on zinc-mediated inhibition of recombinant human SENP1 deSUMOylation activity in the presence of 20 mg/ml albumin. n = 3 independent samples. (two-tailed Student's t-test for pairwise comparisons in l, one-way ANOVA for multiple comparisons in a,b,j,m). ANOVA analyses were subjected to Bonferroni's post hoc test. Data are mean ± s.e.m.

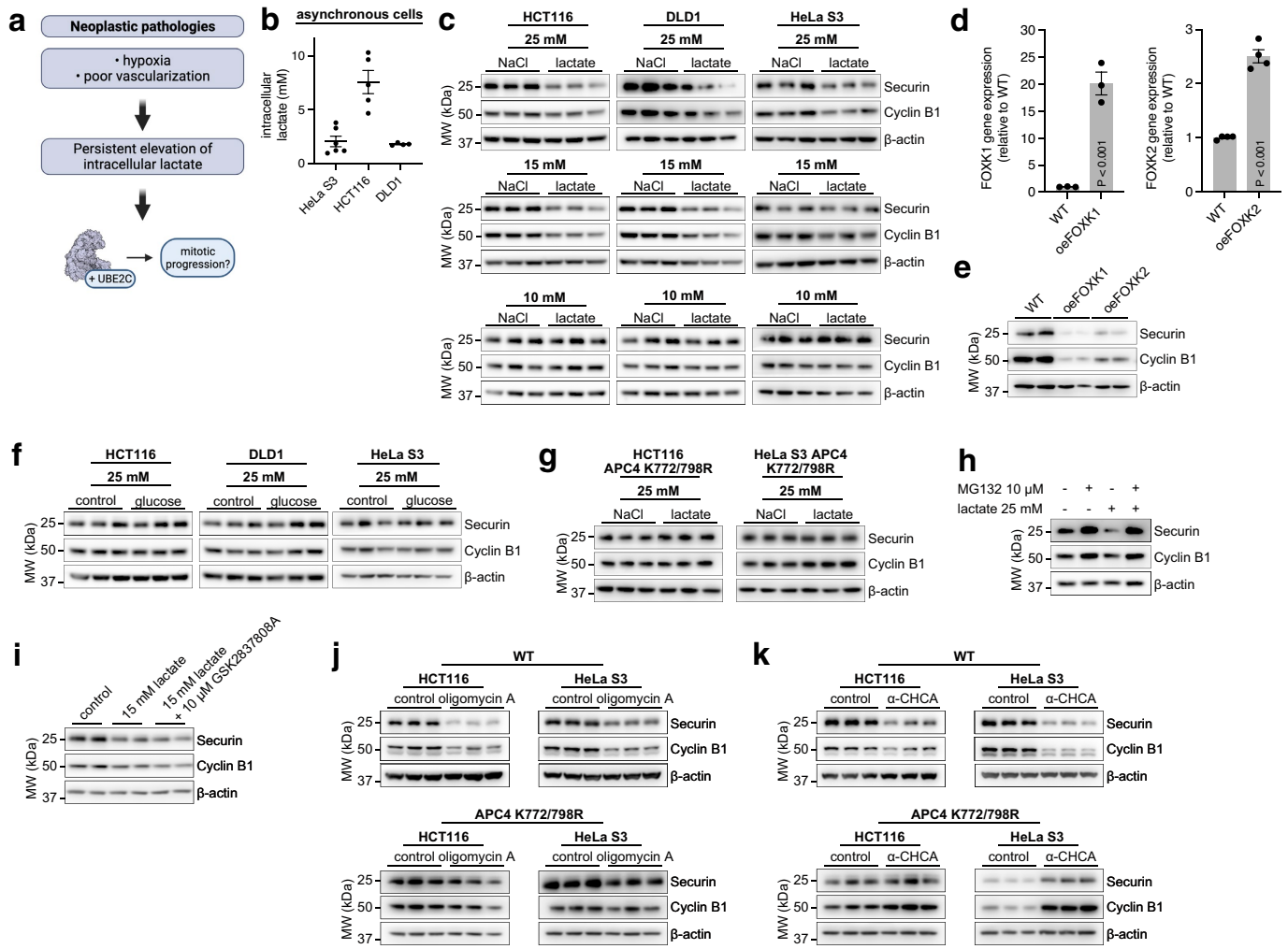


**Extended Data Fig. 5** | See next page for caption.

# Article

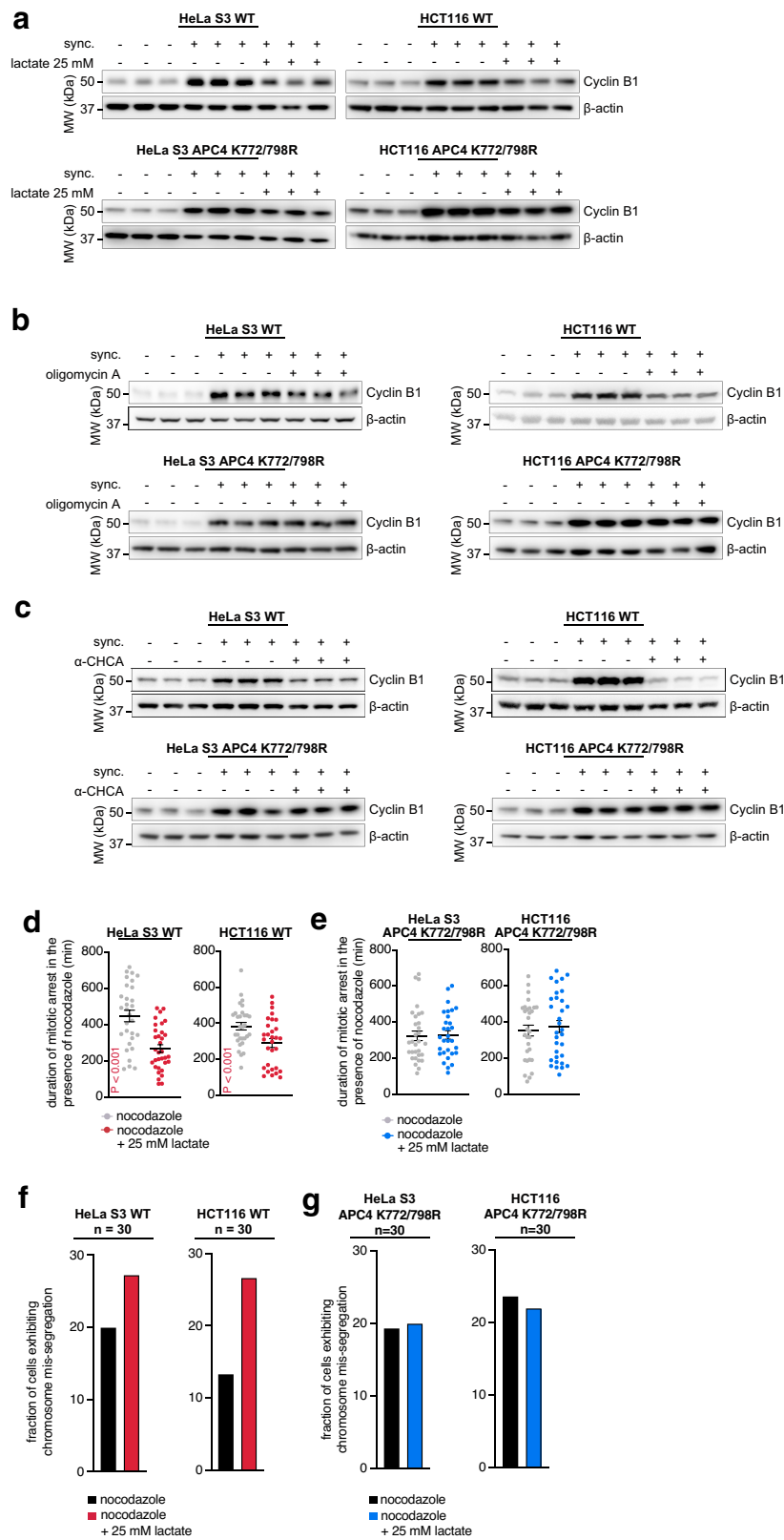
**Extended Data Fig. 5 | Timing and effects of lactate accumulation on cell cycle and proliferation.** (a) Schematic of metabolic flux to anabolic precursors tied to lactate production, pathways predicted to increase flux in response to growth demand in G1/S/G2 phase. (b) Outline of experiment to monitor relationship between lactate abundance and cell cycle phases in proliferative cells. Double thymidine block and release synchronized cells at the G1/S interface as described in Methods. (c) Parallel tracking of securin and cyclin B1 abundance (top), cell cycle phase (middle), and intracellular lactate abundance (bottom) in WT and APC4 K772/798R HCT116 cells. n = 6 cell replicates; 12 h APC4 K772/798R n = 5; lactate abundance n = 6; 6 h WT n = 5. Representative blot from three experiments shown. (d) MS quantification of proteins involved in lactate production and lactate abundance in asynchronous HCT116 cells and 0h, 6h, and 12h post-DTB release. n = 4 cell replicates. (e) MS quantification of lysine lactylation in asynchronous HCT116 cells and 0h, 6h, and 12h post-DTB release. n = 4 cell replicates. (f) Abundance of PDHe1 $\alpha$  and PDHe1 $\alpha$  phosphorylation on residue Ser293 tracked during cell cycle following DTB release. as = asynchronous. Representative blot from three experiments shown. (g) CD8 $^{+}$  T cells stimulated with IL-2 and anti-CD28 for 24 h with cell

cycle and intracellular lactate abundance monitored. Lactate abundance n = 4; cell cycle n = 6 cell replicates. (h) Model for lactate accumulation mediating timed remodeling of APC/C to facilitate mitotic progression. (i)  $\Delta C_t$  quantification of bacterial LMO mRNA expression in HCT116 cells relative to  $\beta$ -actin. n = 3 cell replicates. (j) Cells expressing LMO, or treatment of cells with 25 mM DCA, lowers peak intracellular lactate abundance achieved upon mitotic entry. n = 6 cell replicates. (k) Negative correlation between intracellular lactate abundance and doubling time in 707 human proliferative cancers. See Methods for details. (l) Proliferation rate of WT and APC4 K772/798R HeLa S3 and HCT116 cells. Cells lacking APC4 SUMOylation sites exhibit a significantly lower proliferation rate. n = 4 cell replicates. (m) Exposure of asynchronous HCT116 cells to 1% O<sub>2</sub> for 24 h lowers levels of securin and cyclin B1. Representative blot from three experiments shown. (n) Proliferation rate of WT, APC4 K772/798R, and LMO-expressing HCT116 cells cultured at 1% O<sub>2</sub>. n = 5 cell replicates. (two-tailed Student's t-test for pairwise comparisons in c,j, one-way ANOVA for multiple comparisons in g, two-sided Pearson R in k, two-way ANOVA for multiple comparisons involving two independent variables in l,n). ANOVA analyses were subjected to Bonferroni's post hoc test.



**Extended Data Fig. 6 | Effect of lactate accumulation on cyclin B1, securin, and mitotic exit.** (a) Model for putative role of chronic lactate elevation on APC/C dependent processes in proliferative cells. (b) Intracellular lactate concentration in asynchronous HeLa S3 ( $n = 6$ ), DLD1 ( $n = 4$ ), and HCT116 ( $n = 5$ ) cells.  $n$  indicates cell replicate number. (c) Treatment of asynchronous human proliferative cells with elevated lactate at 15 and 25 mM for 4 h lowers levels of securin and cyclin B1. Representative blot from three experiments shown. (d) mRNA transcript abundance of human FOXK1 ( $n = 3$ ) and FOXK2 ( $n = 4$ ) in HCT116 cells following engineered overexpression (oe).  $n$  designates cell replicates. (e) Effect of forced overexpression on abundance of cyclin B1 and securin in asynchronous HCT116 cells. Representative blot from two experiments shown. (f) Treatment of asynchronous human proliferative cells with elevated glucose for 4 h has no effect on levels of securin and cyclin B1. Representative blot from two experiments shown. (g) Treatment of asynchronous human

proliferative APC4 K772/798R cells with 25 mM lactate for 4 h has no effect on securin or cyclin B1 abundance. Representative blot from three experiments shown. (h) Lactate mediated depletion of securin and cyclin B1 is lost upon treatment with the proteasome inhibitor MG132. Representative blot from three experiments shown. (i) Treatment of asynchronous HCT116 cells with 15 mM lactate for 4 h lowers levels of securin and cyclin B1 in the presence of the LDH inhibitor GSK2837808A. Representative blot from two experiments shown. (j) Effect of treatment of asynchronous human proliferative cells with 1  $\mu$ M oligomycin A for 24 h on abundance of securin and cyclin B1 in WT and APC4 K772/798R cells. Representative blot from three experiments shown. (k) Effect of treatment of asynchronous human proliferative cells with 5 mM  $\alpha$ -CHCA for 24 h on abundance of securin and cyclin B1 in WT and APC4 K772/798R cells. Representative blot from three experiments shown. (two-tailed Student's t-test for pairwise comparisons in d). Data are mean  $\pm$  s.e.m.



**Extended Data Fig. 7** | See next page for caption.

**Extended Data Fig. 7 | Persistent lactate elevation drives mitotic slippage through aberrant APC/C activation.** (a) Treatment of cells with an inhibitor of microtubule assembly nocodazole (sync.) for 14 h to arrest in pro-metaphase leads to accumulation of cyclin B1. Exposure of arrested WT cells to lactate for the last 12 h of nocodazole exposure stimulates depletion of cyclin B1 in the presence of nocodazole. (b) Treatment of HCT116 or HeLa S3 cells with an inhibitor of microtubule assembly nocodazole (sync.) for 14 h to arrest in pro-metaphase leads to accumulation of cyclin B1. Co-exposure of arrested WT cells to 1  $\mu$ M oligomycin A stimulates depletion of cyclin B1 in the presence of nocodazole. Arrested APC4 K772/798R cells treated with oligomycin A exhibit no oligomycin A dependent effect. (c) Treatment of HCT116 or HeLa S3 cells with an inhibitor of microtubule assembly nocodazole (sync.) for 14 h to arrest in pro-metaphase leads to accumulation of cyclin B1. Co-exposure of arrested WT cells to 5 mM  $\alpha$ CHCA stimulates depletion of cyclin B1 in the presence of nocodazole. Arrested APC4 K772/798R cells treated with  $\alpha$ CHCA exhibit no  $\alpha$ CHCA dependent effect. (d,e) Treatment of (d) WT cells and (e) APC4

K772/798R with an inhibitor of microtubule assembly nocodazole for 14 h to arrest in pro-metaphase. Rate of mitotic progression was determined by timelapse microscopy following exposure of cells to lactate for the last 12 h of nocodazole incubation. Analysis represents time in mitotic arrest beginning with nuclear envelope breakdown (NEBD) to DNA decondensation. n = 30 individual cell replicates. (two-tailed Student's t-test for pairwise comparisons in d). (f) Treatment of cells with an inhibitor of microtubule assembly nocodazole for 14 h to arrest in pro-metaphase. Quantification of WT cells exhibiting chromosome mis-segregation following treatment with lactate for the last 12 h of nocodazole exposure. n = 30 individual cell replicates. (g) Treatment of cells with an inhibitor of microtubule assembly nocodazole for 14 h to arrest in pro-metaphase. Quantification of APC4 K772/798R cells exhibiting chromosome mis-segregation following treatment with lactate for the last 12 h of nocodazole exposure. n = 30 individual cell replicates. Data are mean  $\pm$  s.e.m.

## Reporting Summary

Nature Portfolio wishes to improve the reproducibility of the work that we publish. This form provides structure for consistency and transparency in reporting. For further information on Nature Portfolio policies, see our [Editorial Policies](#) and the [Editorial Policy Checklist](#).

### Statistics

For all statistical analyses, confirm that the following items are present in the figure legend, table legend, main text, or Methods section.

n/a Confirmed

- The exact sample size ( $n$ ) for each experimental group/condition, given as a discrete number and unit of measurement
- A statement on whether measurements were taken from distinct samples or whether the same sample was measured repeatedly
- The statistical test(s) used AND whether they are one- or two-sided
  - Only common tests should be described solely by name; describe more complex techniques in the Methods section.*
- A description of all covariates tested
- A description of any assumptions or corrections, such as tests of normality and adjustment for multiple comparisons
- A full description of the statistical parameters including central tendency (e.g. means) or other basic estimates (e.g. regression coefficient) AND variation (e.g. standard deviation) or associated estimates of uncertainty (e.g. confidence intervals)
- For null hypothesis testing, the test statistic (e.g.  $F$ ,  $t$ ,  $r$ ) with confidence intervals, effect sizes, degrees of freedom and  $P$  value noted
  - Give  $P$  values as exact values whenever suitable.*
- For Bayesian analysis, information on the choice of priors and Markov chain Monte Carlo settings
- For hierarchical and complex designs, identification of the appropriate level for tests and full reporting of outcomes
- Estimates of effect sizes (e.g. Cohen's  $d$ , Pearson's  $r$ ), indicating how they were calculated

*Our web collection on [statistics for biologists](#) contains articles on many of the points above.*

### Software and code

Policy information about [availability of computer code](#)

Data collection Gen5 3.10 software was used for imaging experiments, graphpad prism, and excel for data collection.

Data analysis Microsoft excel, and prism were used for numerical data analysis, plotting, and statistics.

For manuscripts utilizing custom algorithms or software that are central to the research but not yet described in published literature, software must be made available to editors and reviewers. We strongly encourage code deposition in a community repository (e.g. GitHub). See the Nature Portfolio [guidelines for submitting code & software](#) for further information.

### Data

Policy information about [availability of data](#)

All manuscripts must include a [data availability statement](#). This statement should provide the following information, where applicable:

- Accession codes, unique identifiers, or web links for publicly available datasets
- A description of any restrictions on data availability
- For clinical datasets or third party data, please ensure that the statement adheres to our [policy](#)

Mass spectrometry proteomics data have been deposited to the ProteomeXchange Consortium via the PRIDE partner repository with the dataset identifier PXD036641. NMR backbone resonance assignments of SENP1 are deposited to the BRMB and can be accessed with the accession code 51766. All other data associated with this work will be provided upon request to the corresponding author.

# Field-specific reporting

Please select the one below that is the best fit for your research. If you are not sure, read the appropriate sections before making your selection.

Life sciences

Behavioural & social sciences  Ecological, evolutionary & environmental sciences

For a reference copy of the document with all sections, see [nature.com/documents/nr-reporting-summary-flat.pdf](https://nature.com/documents/nr-reporting-summary-flat.pdf)

## Life sciences study design

All studies must disclose on these points even when the disclosure is negative.

Sample size	Sample sizes were determined based on previous experiments using similar methodologies to account for relevant biological and technical variability, then estimating statistical power based on methods described in PMID 12391396
Data exclusions	No data was excluded
Replication	All experimental findings were reproduced as biological replicates as the value stated in the figure legend, unless otherwise indicated. All additional replication attempts were successful.
Randomization	For MS, and cell cycle experiments, samples were processed in random order and experimenters were blinded to experimental condition, and sample allocation was randomized
Blinding	For MS, and cell cycle experiments, samples were processed in random order and experimenters were blinded to experimental condition. For other experiments the investigator was not blinded since the same individual performed and analyzed experimental data.

## Reporting for specific materials, systems and methods

We require information from authors about some types of materials, experimental systems and methods used in many studies. Here, indicate whether each material, system or method listed is relevant to your study. If you are not sure if a list item applies to your research, read the appropriate section before selecting a response.

### Materials & experimental systems

n/a	Involved in the study
<input type="checkbox"/>	<input checked="" type="checkbox"/> Antibodies
<input type="checkbox"/>	<input checked="" type="checkbox"/> Eukaryotic cell lines
<input checked="" type="checkbox"/>	<input type="checkbox"/> Palaeontology and archaeology
<input checked="" type="checkbox"/>	<input type="checkbox"/> Animals and other organisms
<input checked="" type="checkbox"/>	<input type="checkbox"/> Human research participants
<input checked="" type="checkbox"/>	<input type="checkbox"/> Clinical data
<input checked="" type="checkbox"/>	<input type="checkbox"/> Dual use research of concern

### Methods

n/a	Involved in the study
<input checked="" type="checkbox"/>	<input type="checkbox"/> ChIP-seq
<input checked="" type="checkbox"/>	<input type="checkbox"/> Flow cytometry
<input checked="" type="checkbox"/>	<input type="checkbox"/> MRI-based neuroimaging

## Antibodies

### Antibodies used

cdc27 (AF3.1) (Santa Cruz, sc-9972)  
 APC4 (Bethyl Laboratories, A301-176A)  
 UBE2C (Abcam, ab252940)  
 anti-rabbit HRP (Promega, W401B)  
 anti-mouse HRP (Promega, W402B)  
 SUMO2/3 (Abcam, ab81371)  
 Cyclin B1 (CST, #12231)  
 Securin (CST, 13445)  
 SUMO1 (PTM BIO, PTM-6055)  
 SENP1 (Proteintech, 25349-1-AP)  
 CDC27 (Santa Cruz, sc-9972)  
 H3 (CST, 4499)  
 phos-H3S10 (CST, 53348)  
 PDH (CST, 3205)  
 phos-PDH(CST, 31866)  
 β-actin (CST, 3700))

### Validation

Above antibodies have all been validated by manufacturer. In addition, we validated APC4 (ED Figure 2H) and SENP1 (ED Figure 2j) antibodies using KO controls in the paper.

## Antibody validation sources:

cdc27 (AF3.1) (Santa Cruz, sc-9972) - <https://www.scbt.com/p/cdc27-antibody-af3-1>  
APC4 (Bethyl Laboratories, A301-176A) - <https://www.thermofisher.com/antibody/product/APC4-Antibody-Polyclonal/A301-176A>  
UBE2C (Abcam, ab252940) - <https://www.abcam.com/ube2c-antibody-epr23165-31-ab252940.html>  
anti-rabbit HRP (Promega, W401B) - <https://www.promega.com/products/protein-detection/primary-and-secondary-antibodies/anti-rabbit-igg-h-and-l-hrp-conjugate/>  
anti-mouse HRP (Promega, W402B) - [https://www.promega.com/products/protein-detection/primary-and-secondary-antibodies/anti\\_mouse-igg-h-and-l-hrp-conjugate/?catNum=W4021](https://www.promega.com/products/protein-detection/primary-and-secondary-antibodies/anti_mouse-igg-h-and-l-hrp-conjugate/?catNum=W4021)  
SUMO2/3 (Abcam, ab81371) - <https://www.abcam.com/sumo-2--sumo-3-antibody-8a2-ab81371.html>  
Cyclin B1 (CST, #12231) - [https://www.cellsignal.com/product/productDetail.jsp?productId=12231&utm\\_medium=b2b&utm\\_campaign=general](https://www.cellsignal.com/product/productDetail.jsp?productId=12231&utm_medium=b2b&utm_campaign=general)  
Securin (CST, 13445) - <https://www.cellsignal.com/products/buy-3-get-4th-free/primary-antibodies/securin-d2b6o-rabbit-mab/13445>  
SUMO1 (PTM BIO, PTM-6055) - <https://www.ptmbiolabs.com/product/anti-sumo1-rabbit-mab-ct/>  
SENP1 (Proteintech, 25349-1-AP) - <https://www.ptglab.com/products/SENP1-Antibody-25349-1-AP.htm>  
H3 (CST, 4499) - <https://www.cellsignal.com/products/primary-antibodies/histone-h3-d1h2-xp-rabbit-mab/4499>  
phos-H3S10 (CST, 53348) - <https://www.cellsignal.com/products/primary-antibodies/phospho-histone-h3-ser10-d7n8e-xp-rabbit-mab/53348>  
PDH (CST, 3205) - <https://www.cellsignal.com/products/primary-antibodies/pyruvate-dehydrogenase-c54g1-rabbit-mab/3205>  
phos-PDH(CST, 31866) - <https://www.cellsignal.com/products/primary-antibodies/phospho-pyruvate-dehydrogenase-a1-ser293-antibody/31866>  
β-actin (CST, 3700) - <https://www.cellsignal.com/products/primary-antibodies/b-actin-8h10d10-mouse-mab/3700>

## Eukaryotic cell lines

Policy information about [cell lines](#)

Cell line source(s)	ATCC: HeLa S3, HCT116, DLD1, HEK293
Authentication	Validated by ATCC using STR profiling: <a href="https://www.atcc.org/en/services/cell-authentication">https://www.atcc.org/en/services/cell-authentication</a>
Mycoplasma contamination	Cells tested negative for mycoplasma.
Commonly misidentified lines (See <a href="#">ICLAC</a> register)	None used here